ANALYSIS OF CRACK INITIATION IN EDGE CRACKED NITI SHAPE MEMORY ALLOY PLATE

by

Onat Baykara

B.S., Mechanical Engineering, Polytechnic University of Turin, 2018

Submitted to the Institute for Graduate Studies in
Science and Engineering in partial fulfilment of
the requirements for the degree of
Master of Science

Graduate Program in Mechanical Engineering
Boğaziçi University

2022

ACKNOWLEDGEMENTS

First of all, I would like to thank my thesis advisor Assist. Prof. Sertan Alkan for his great support during my study in terms of both teaching and leading the way. I would like to express my gratitude to the committee members Prof. Günay Anlaş and Assist. Prof. Alpay Oral for their valuable comments and encouragement.

I have to thank my friends, Bilge Yavuzyiğit, Seda Anbar, Bedri Seyhan, Barış Gökçe, Arda Şafak and Baran Ataman, who supported me during my study and without their encouragement, I would not be able to finish my thesis.

A special thanks to my colleagues and managers at Tekfen, they always provided the time that I need to finish my thesis for 3 years.

Finally, I am a lucky person to have such a family who always supported me without questioning anything, thanks to my father, mother and sister.

ABSTRACT

ANALYSIS OF CRACK INITIATION IN EDGE CRACKED NITI SHAPE MEMORY ALLOY PLATE

Shape Memory Alloys (SMAs) are getting more known among scientist and the engineers day by day. Therefore, their industrial, military and also daily life applications are increasing. Their unique properties make them very useful under special circumstances, however also because of that, there are some parameters (such as fracture), behaviors that need to be discovered. This thesis is designed to investigate the fracture behavior of the Shape Memory Alloys. Their super elastic behavior and martensitic transformation, especially around crack tip, is modeled on ABAQUS software followed by some MATLAB fitting evaluations in order to implement data to conventional fracture criterions. The different material properties are changed and their effects on crack angles are studied. As a result of simulations, effect of every material property and crack angle change is discussed on the last chapter. The results are interpreted as the martensitic transformation effects the crack angle according to MTS, Det and Ip crack initiation criterions due to strain hardening.

ÖZET

NITI ŞEKİL HAFIZALI ALAŞIM (ŞHA) PLAKANIN KENAR ÇATLAK BAŞLANGICI ANALİZİ

Şekil Hafızalı Alaşımlar (SHA'lar) gün geçtikçe bilim adamları ve mühendisler tarafından daha fazla tanınmakta ve endüstriyel, askeri ve ayrıca günlük yaşam uygulamaları artmaktadır. Benzersiz özellikleri sayesinde özel şartlarda kullanılabilmektedirler, ancak bu benzersiz özellikler ile ilgili keşfedilmesi gereken bazı parametreler (kırılma gibi), davranışlar vardır. Bu tezde, şekil hafızalı alaşımların kırılma davranışları incelenmiştir. Malzemelerin süperelastik davranışları ve martensitik dönüşümleri, özellikle çatlak ucu etrafında, ABAQUS programı kullanılarak modellenmiştir. Elde edilen veriler, MATLAB programı kullanılarak sürekli bir fonksiyon haline getirilmiş, geleneksel kırılma kriterlerine uygun olarak değerlendirilmiştir. Araştırmada farklı malzemeler kullanılmış ve malzeme özelliklerinin çatlak açıları üzerindeki etkileri incelenmiştir. Simülasyonlar sonucunda her malzeme özelliğinin etkisi ve çatlak açısı değişimi son bölümde değerlendirilmiştir. Sonuç olarak, martensitik dönüşümün, gerilme sertleşmesi nedeniyle MTS, Det ve Ip çatlak ilerleme kriterlerine göre çatlak açısını etkilediği kanısına varılmıştır.

TABLE OF CONTENT

LIST OF FIGURES

LIST OF TABLES

LIST OF SYMBOLS

A	Area
A_F	Austenitic final temperature
A_S	Austenitic start temperature
E_A	Young's modulus of austenite
E_M	Young's modulus of martensite
F_ζ^f	Forward transformation function of phase change
F_ζ^r	Reverse transformation function of phase change
G	Energy release rate
G_{tr}	Transformation flow potential
J	J-Integral
K_{TIP}	Crack tip SIF
K_C	Fracture toughness
K_{eff}	Effective SIF
K_{APP}	Far-field SIF
K_{TRAN}	SIF change due to transformation
M_d	Martensite desist temperature
M_f	Martensite final temperature
M_s	Martensite start temperature
n	Hardening coefficient
S	Strain energy density factor
SS	Sum of squares
T	Temperature
W_s	Total energy required for creating new surfaces
ν	Poisson's ratio
$\Delta\varepsilon$	Strain increment
ζ	Martensite fraction
π	Potential energy of the applied loading
ρ	Length of plastic zone end of the crack tip

σ^{AF}	Austenite finish stress
σ^{AS}	Austenite start stress
σ^{MF}	Martensite finish stress
σ^{MS}	Martensite start stress
σ_{ij}	Cauchy stress tensor
σ_{ij}^{d}	Deviatoric part of stress tensor

LIST OF ABBREVIETIONS AND ACRONYMS

2D	Two Dimensional
CPS8R	Eight Node Plane Stress Element
FE	Finite Element
FEA	Finite Element Analysis
FEM	Finite Element Method
HRR	Hutchinson-Rise-Rosengren
LEFM	Linear Elastic Fracture Mechanics
Lsqnonlin	Least Square Non-Linear
MTS	Maximum Tangential Stress
MVF	Martensite Volume Fraction
NiTi	Nickel Titanium Alloy
NOL	Naval Ordnance Laboratory
SIF	Stress Intensity Factor
SIM	Simulation
SMA	Stress Memory Alloy
SME	Stress Memory Effect
ŞHA	Şekil Hafızalı Alaşım

1. INTRODUCTION

Shape Memory Alloys (SMAs) are a special class of alloy systems which can remember their original configuration after being exposed to either thermal or mechanical stimulus. The discovery of reversible martensitic transformable materials started with NiTi alloy and it was named as NITINOL (Nickel Titanium- Naval Ordnance Lab)[1]. However, the phenomenon under such behavior is discovered by Miyazaki et al., 1982 [2]. Further studies made scientists and engineers study on cheaper and easily manufacturable SMAs and so Cu based SMAs such as CuZn, CuZnAl, CuAlNi are discovered [3]. In addition to that, how inclusion of new elements such as Ni, Cu, Co, Al affects the SME is still studied [4]. This memory property is associated with diffusionless, martensitic phase transformation in which a high symmetry austenite (A) crystal structure undergoes through a transition to low symmetry martensite (M) phase. Within the last three decades, this class of alloys have attracted remarkable attention in a vast range of engineering applications in aerospace (torque tubes, variable geometry chevron) [5], construction (seismic isolation devices, hybrid structures) [6], biomedical (orthodontic wires, aortic valves, implants) [7], automotive (smart suspension, active aerodynamic spoilers) [8] industries as well as sensor technologies (activated either by pressure or temperature change) [9].

The wide range engineering applications employing SMAs necessitate high functional performance quantified based on the reversibility of large martensitic transformation strains (on the order of 2-5%) in a prescribed temperature and applied stress interval. The transformation response of an SMA system is characterized by its Gibbs free energy in a given range of service temperature and stress levels [10]. Considering the fact that Gibbs free energy is dependent on temperature and stress as externally controlled variables for a given composition of an SMA system, the following critical quantities are introduced below to describe the initiation and end of forward (A to M) and reverse (M to A) transformation state.

The reversible transformation mechanisms are clustered into two main behaviors: (i) shape memory effect (SME) and (ii) pseudoelasticity. Meanwhile, SME is used to generate reversible transformation mainly through a thermomechanical cycle spanning a temperature

range of $A_F - M_f - A_F$; pseudoelasticity mechanism is exploited primarily above AF temperature with a loading cycle spanning $\sigma^{MS} - \sigma^{MF} - \sigma^{AS} - \sigma^{AF}$ stresses. As the performance of SMAs are directly dependent on these variables, the subsequent subsections are devoted to detail SME and pseudoelasticity.

1.1. SME

Shape Memory Effect (SME) is observed on loading path below M_F (so at martensitic phase), followed by heating above A_F. Below, Figure 1.1 shows a thermomechanical path exhibiting SME. At point I, twinned martensite is present from A to M phase transformation induced by cooling. Loading path (1-2), consists of significant strain levels owing to detwinned martensite [11]. Unloading through path (2-3) introduces elastic recovery. However, as can be distinguished by the points III and I, the detwinning strain persists at zero loading. Upon heating above Af temperature, the austenite crystal is favored which recovers the substantial portion of the strain quantified by the difference between III and I [12].

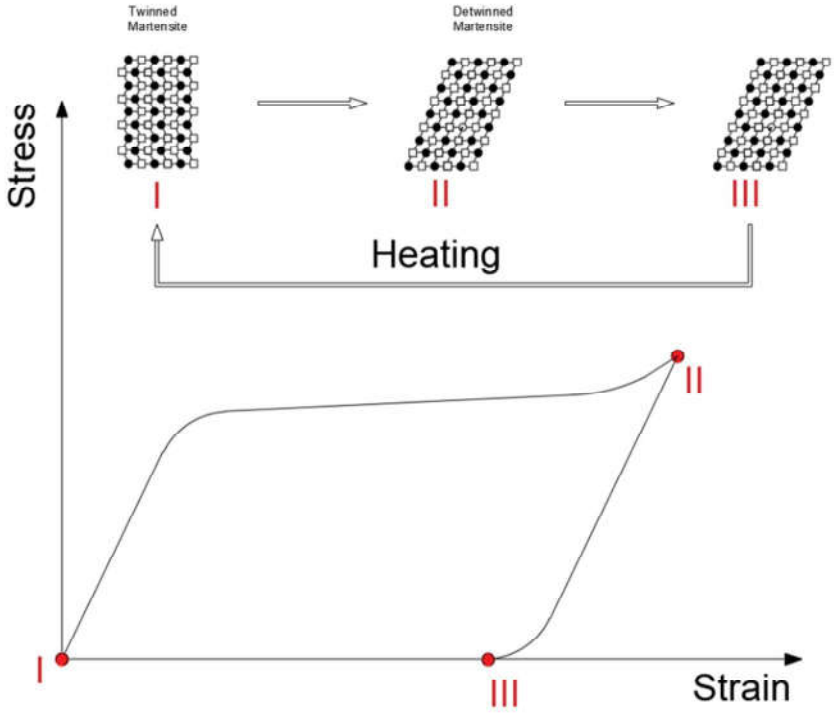

Figure 1.1. The crystallographic changes due to the SME.

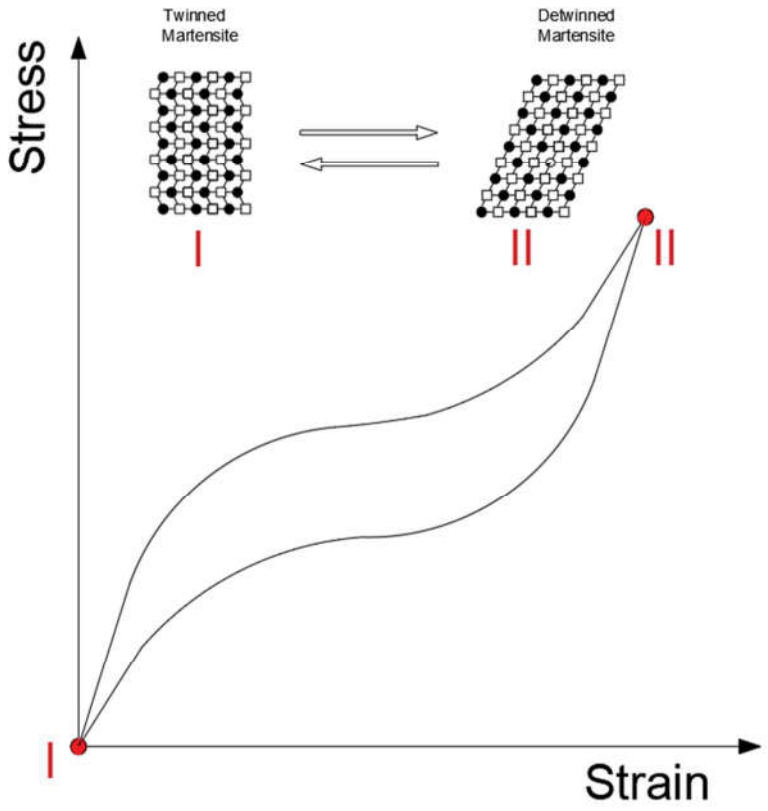

Figure 1.2. Pseudo elastic response under loading above Mf.

1.2. Pseudoelasticity

Pseudoelasticity phenomenon is another stress induced martensitic transformation strain recovery mechanism observed at constant temperature above Af as illustrated in Figure 1.2. On loading path (I-II), material crosses the critical transformation stress, σ^{MS}, (at the start of the plateau) and the martensitic transformation initiates. Further loading after this point, increases martensite volume fraction. At point II, a microstructure of fully transformed martensite phase is observed [13,14].

Interestingly upon unloading, the transformation strain is recovered since the austenitic transformation occurs starting from the beginning of the plateau indicated by austenite start stress, σ^{AS} to the final point of austenite finish stress, σ^{AF}. As can be distinguished in Figure 1.2, there is a difference in stress levels associated with 50% martensite volume fraction which corresponds to approximately mid-portions of forward & reverse transformation plateaus. It is describing the energy dissipation upon the full cycle.

The present study primarily aims to focus on the incorporation of the reversible martensitic transformation response of SMAs to the development of a predictive tool to quantify the crack initiation phenomenon in edge cracked two dimensional configurations, particularly focusing on NiTi alloy.

1.3. Fracture Mechanics Concepts

As our primary purpose is to establish an understanding on crack extension criterion for SMAs, in the present study, we would like to briefly introduce the fundamental concepts in fracture mechanics. The stress field around the crack tip is calculated based on Williams's [15] asymptotic expansion as follows:

$$\sigma_{ij} = \left(\frac{k}{\sqrt{r}}\right) f_{ij}(\theta) + \sum_{n=0}^{\infty} \left(A_n r^{\frac{n}{2}} g_{ij}^{(n)}(\theta)\right), \tag{1.1}$$

where, stress is proportional to $1/\sqrt{r}$ term and other terms in sum formula are approaching to 0 near the crack tip. The term governing on $1/\sqrt{r}$ is strongly dependent on the geometric configurations of the crack and applied loading far field. As illustrated in Figure 1.3, the possible configurations can be grouped into three cases as follows[16]:

(i) Mode I (opening),
(ii) Mode II (in plane shear),
(iii) Mode III (out of plane shear).

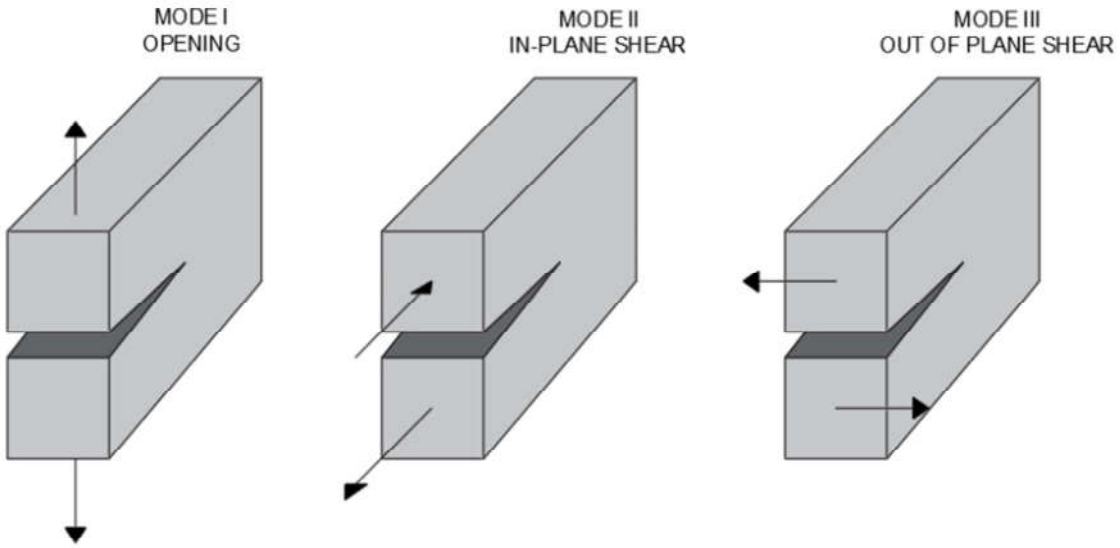

Figure 1.3. Schematic representation of three modes of loading.

By introducing stress intensity factor, K=k$\sqrt{2\pi}$ expressed as for different modes, the stress fields at the tip of the crack are

$$\lim_{r\to\infty} \sigma_{ij}^{(I)} = \frac{K_I}{\sqrt{2\pi r}} f_{ij}^{(I)}(\theta) \tag{1.2}$$

$$\lim_{r\to\infty} \sigma_{ij}^{(II)} = \frac{K_I}{\sqrt{2\pi r}} f_{ij}^{(II)}(\theta) \tag{1.3}$$

$$\lim_{r\to\infty} \sigma_{ij}^{(III)} = \frac{K_I}{\sqrt{2\pi r}} f_{ij}^{(III)}(\theta). \tag{1.4}$$

The coordinate frame used in Equation (1.1) to Equation (1.4) is attached to crack tip as illustrated in Figure 1.4. Note that the stress field ahead of the crack tip in Figure 1.4 corresponds to σ_{yy} in Mode I. The asymptotic response can be clearly distinguished. Similar trends are exhibited by also Mode II and Mode III. At this stage, it should be noted that the K term is a function of both applied loading and geometry.

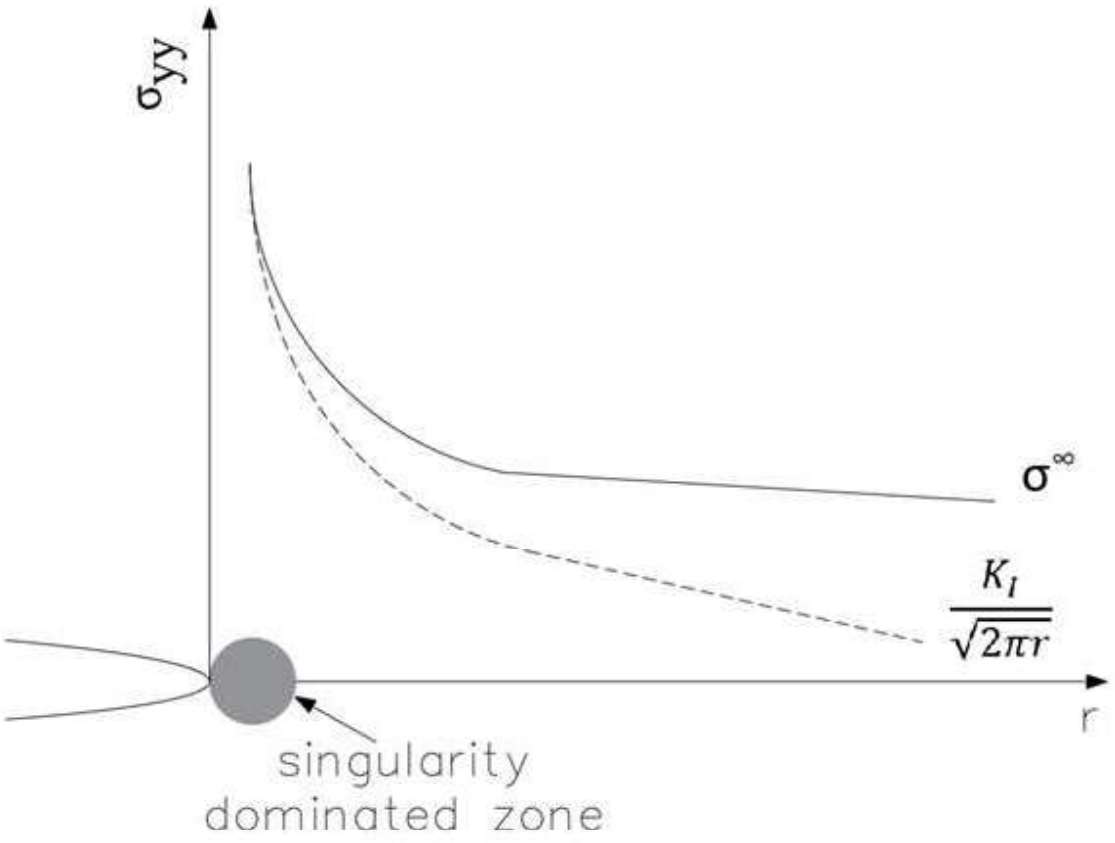

Figure 1.4. Stress-Radius graph for Mode I loading.

1.4. Energy Approach for Crack Advance Predictions

Meanwhile, we have derived the stresses acting at the crack tip, we proposed no criterion for crack extension, yet. On this basis, thermodynamical analysis of the crack tip advance phenomenon stands out as a necessity. This is in fact what Griffith has put forward with his prominent work on fracture of glass whiskers [17]. In his work, the total energy, E, of the closed system composed of a cracked plate with a crack site of 2a, the potential energy of the applied loading, denoted as π and W_s is the total energy required for creating new surfaces on the following equation:

$$\frac{dE}{dA} = \frac{d\pi}{dA} + \frac{dW_s}{dA} = 0. \qquad (1.5)$$

Equation (1.5) denotes that the total energy charge associated with an infinitesimal crack size increase is composed of the total potential energy of applied loading and the crack surfaces generated, W_s, neglecting plasticity effects. Note that in Equation (1.5), dA is projected crack area increment which is expressed as

$$\mathrm{dA} = 2\mathrm{Bda}, \tag{1.6}$$

where B is the thickness. Noting that, $W_s = 4aB\gamma_s$ with γ_s is equal to surface energy per crack area, then the potential energy release rate denoted as $-\frac{d\pi}{da}$ is expressed as:

$$G = -\frac{d\pi}{dA} = 2\gamma_s, \tag{1.7}$$

where *G* is employed to honor Griffith. The above Equation (1.7) dictates that the critical driving force is governed by *G* term. Meanwhile *G* is utilized to quantify the tendency of the applied loading to extend a crack in a given configuration, the physical crack advancement occurs only when *G* term reaches a critical value which is named as G_c is a metric to be determined by experimental measurements.

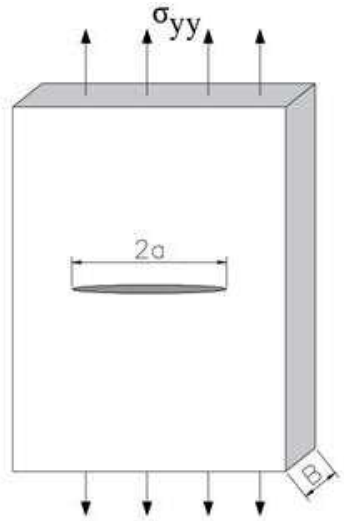

Figure 1.5. A through crack in an infinitely wide plate under tensile stress.

1.5. Plasticity Effects on Crack Tip Fracture Behavior

So far, the fracture mechanics principles introduced are focusing on brittle fracture where no plastic deformation around the crack tip is considered. On the other hand, in ductile materials such as SMAs, the transformation induced deformation is similar to the plasticity suppressed the stress fields at the crack tip. To this end, the conventional linear elastic fracture mechanics (LEFM) should be modified. Below, the well-established models from the earlier literature have been discussed briefly.

1.5.1. Irwin Approach

The Irwin Approach aims to evaluate elastic-plastic boundary [18]. This boundary can be expressed as

$$\sigma_{YS} = \sigma_{yy} \tag{1.8}$$

$$\sigma_{YS} = \frac{K_I}{\sqrt{2\pi r_y}} \tag{1.9}$$

$$r_y = \frac{1}{\sqrt{2\pi}}\left(\frac{K_I}{\sigma_{YS}}\right)^2, \tag{1.10}$$

where r_y is plastic zone radius and σ_{YS} is yield strength obtained under tensile loading.

As a modification, the redistribution of stress when yielding occurs to obtain equilibrium is included in Modified Irwin's Approach. Since stress cannot exceed the σ_{YS}in the elastic-plastic approach, forces which are present at stress values higher than σ_{YS} are used to obtain elastic-plastic behavior [19]. Such a stress field increases the plastic zone as shown in Figure 1.6 and equilibrium of elastic and elastic-plastic approach is as follows [20]

$$\sigma_{YS} r_P = \int_0^{r_y} \frac{K_I}{\sqrt{2\pi r}}\, dr \tag{1.11}$$

and by solving for r_p is by using Equation (1.11),

$$r_p = \frac{1}{\pi}\left(\frac{K_I}{\sigma_{YS}}\right)^2, \tag{1.12}$$

where r_p denotes the corrected plastic zone.

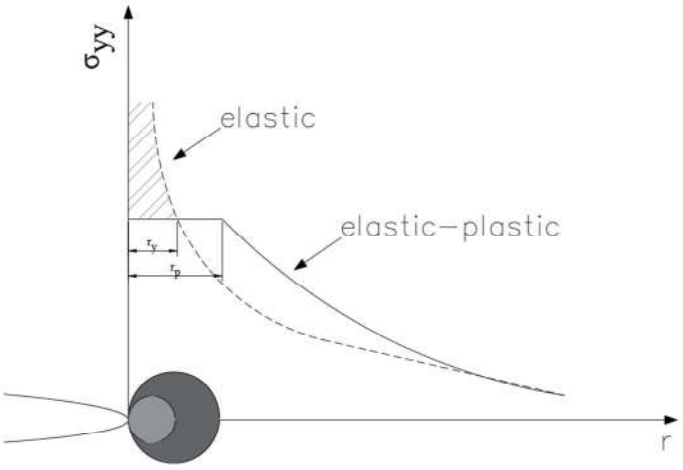

Figure 1.6. Representation of plastic zone size (r_y, r_p).

Based on this rationale, Irwin corrected the crack length by adding plastic zone correction and introducing a_{eff},

$$a_{eff} = a + r_y. \tag{1.13}$$

The effective crack length naturally brings up the concept of effective stress intensity K_{eff} defined as

$$K_{eff} = Y(a_{eff})\sigma\sqrt{\pi a_{eff}}, \tag{1.14}$$

where Y is the geometric correction factor, which conveys the finite size boundary effect information. An iterative solution scheme is employed to determine K*eff*.

1.5.2. The Strip Yield Approach

The strip yield model is studied on through crack 2a+2ρ length (where ρρ is the length of plastic zone end of the crack tips as shown in Figure 1.7). The plastic zone length, ρ, is the distance which remote tension and closure stresses are equal. Due to finite stresses formed of the crack tip, stress singularity is not present, which means the $1/\sqrt{r}$ term is zero. The stress intensity of unit thickness plate due to load P at a distance x from the crack is given by [21, 22]

$$K_{1(+a)} = \frac{P}{\sqrt{\pi a}}\sqrt{\frac{a+x}{a-x}} \tag{1.15}$$

$$K_{1(-a)} = \frac{P}{\sqrt{\pi a}}\sqrt{\frac{a-x}{a+x}}, \tag{1.16}$$

where P is

$$P = -\sigma_{YS}dx. \tag{1.17}$$

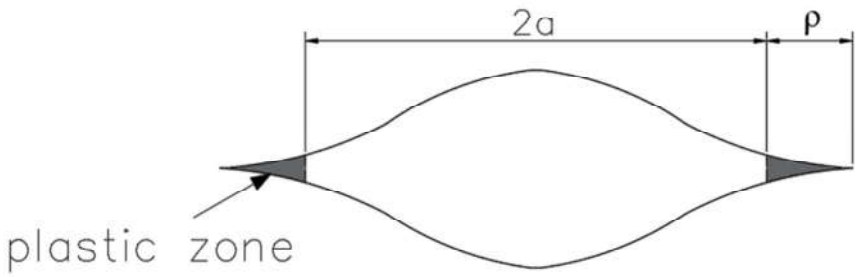

Figure 1.7. The strip yield model plastic zone representation.

The total stress intensity is evaluated by summing the effect of both crack tips [24]

$$K_{closure} = -\frac{\sigma_{YS}}{\sqrt{\pi(a+\rho)}}\int_{a}^{a+\rho}\left\{\sqrt{\frac{a+p+x}{a+p-x}}+\sqrt{\frac{a+p-x}{a+p+x}}\right\}dx, \quad (5)$$

which simplifies to

$$K_{closure} = -2\sigma_{YS}\sqrt{\frac{a+p}{\pi}}\cos^{-1}\left(\frac{a}{a+\rho}\right). \quad (1.19)$$

Noting that the stress intensity induced by the remote tensile ($K_\sigma = \sigma\sqrt{\pi(a+\rho)}$) should be equal to $K_{closure}$, then:

$$\frac{a}{a+\rho} = \cos\frac{\pi\sigma}{2\sigma_{YS}}. \quad (1.20)$$

Further simplification by using the first two terms of the Taylor Series of the cosine term in the above equation leads to an explicit expression for *P*:

$$\rho = \frac{\pi^2\sigma^2 a}{8\sigma_{YS}^2} = \frac{\pi}{8}\left(\frac{K_1}{\sigma_{YS}}\right)^2. \quad (1.21)$$

Then effective stress intensity factor turns out to be

$$K_{eff} = \sigma_{YS}\sqrt{\pi a}\left[\frac{8}{\pi^2}\ln\sec\left(\frac{\pi\sigma}{2\sigma_{YS}}\right)\right]^{1/2}. \quad (1.22)$$

1.5.3. J-Integral

In order to define the energy that is released with the crack extension, a contour integral called J-Integral is introduced by Rice [25].

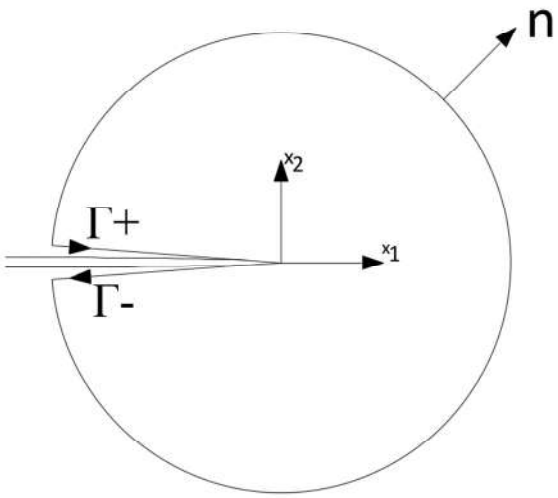

Figure 1.8. J-Integral representation, contour directions and n vector.

The J-Integral is defined as

$$J = \int_{\Gamma} \left(w dy - T_i \frac{\partial u_i}{\partial x} ds \right), \tag{1.23}$$

where w is the strain energy density, T_i are components of the traction vector, u_i are the displacement vector components and ds is a length increment along the contour Γ-. Counter-clockwise path (Γ-) is defined as shown in Figure 1.8.

The potential energy of system (Π) is defined as follows under quasistatic conditions and in the absence of body forces,

$$\Pi = \int_{A'} w dA - \int_{\Gamma'} T_i u_i ds \tag{1.24}$$

and the change in potential energy is as follows

$$\frac{d\Pi}{da} = \int_{A'} \frac{dw}{da} dA - \int_{\Gamma'} T_i \frac{du_i}{da} ds. \tag{1.25}$$

By using principle of virtual work and Green's theorem, the derivations tend to

$$-\frac{d\Pi}{da} = \int_{\Gamma'} \left(w n_x - T_i \frac{du_i}{dx} \right) ds, \tag{1.26}$$

where $n_x ds = dy$. To sum up, for elastic materials, the J-integral is equal to the energy release rate.

Rice showed that the J-Integral is path-independent for a homogeneous elastic material [25]. For a linear elastic homogeneous material, the J-integral value is equal to *G* and therefore can be linked to the stress intensity factors. In contrast, in the presence of plasticity effects, the path-independent character of J-integral can be exploited only by mimicking the proportional loading elastic-plastic constitutive response by a non-linear elastic response. Though, J-integral based fracture response characterization is frequently used in the presence of plasticity. In the particular case of SMAs, as the martensitic fields are analogous to plastic deformation for monotonic loading, J-integral controlled fracture mechanics techniques can be still adapted.

1.6. Fracture Mechanics of Shape Memory Alloys

In SMA systems, due to martensitic phase transformation, elastic or elastic plastic theories cannot directly be adopted. In this case, a modified LEFM model should be considered to analyze behavior of such materials which can capture the transformation effects minimizing elastic-plastic response. In the earlier literature, analytical model, FEA and experimental approaches are designed and compared to obtain response of modified stress intensity factors [26].

1.6.1. Asymptotic Analytical Models

This work is originally conducted by Maletta et al. [27]. at the crack tip zone, in which three different regions are defined as martensitic region, transformation region and austenitic region as illustrated in Figure 1.9. Large strain caused by martensitic deformation and the elastic misfit make improper use of common LEFM methods. For such condition, a

modified LEFM method which regards the forward transformation within the framework of deformation plasticity is proposed.

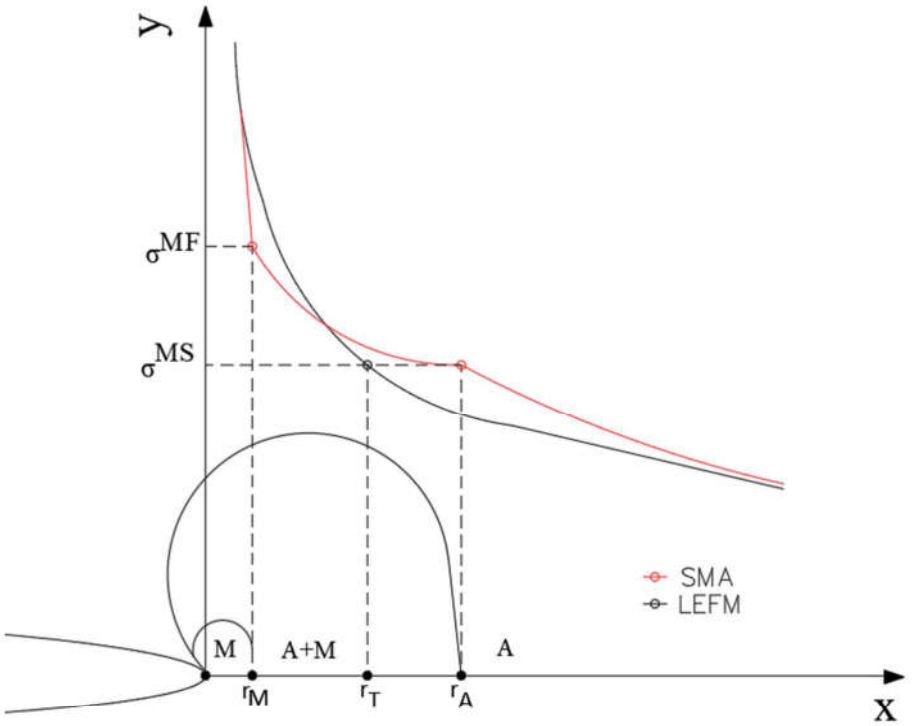

Figure 1.9. Crack tip stress distribution and transformation region for SMA.

In this approach for austenitic region near the crack tip, the following explicit formula proposed to evaluate the principal stress components,

$$\sigma_{Ai}(r) = g_i \frac{K_{Ie}}{\sqrt{2\pi(r-\Delta r)}}, \qquad (1.27)$$

where i=1,2,3 and g_i=1 for i=1,2 and g_i=b for i=3 with b=0 for plane stress and $b=2v$ for under plane strain conditions. In Equation (1.27) K_{Ie} term stands for an effective stress intensity factor value.

Similarly, for martensitic region, the principal stress components are captured by a more involved expression:

$$\sigma_{Mi}(r) = g_i \frac{2(1+v+bv)K_{Ie}/\sqrt{2\pi r} - E_A\varepsilon_L + \alpha_M^{-1}\sigma_f^{AM} - \sigma_s^{AM}}{(1-b)\alpha_M^{-1} + (b+1)(1-2v)}. \quad (1.28)$$

In this problem, the site of the totally martensitic region is also significant and it is characterized as:

$$r_M = \frac{2}{\pi}\left(\frac{(1-v-bv)(1-b)K_{Ie}}{(1-b)E_A\varepsilon_L + (b+1)(1-2v)\sigma_f^{AM} + (1-b)\sigma_s^{AM}}\right)^2. \quad (1.29)$$

Finally, along with principle stress formulas both for martensitic and austenitic regions, stress intensity factor for austenitic region is calculated as follows:

$$K_{IA} = \lim_{\tilde{r}\to 0}\sqrt{2\pi\tilde{r}}\sigma_A = K_{Ie}\,, \quad (1.30)$$

and for martensitic region is calculated as follows:

$$K_{IM} = \lim_{r\to 0}\sqrt{2\pi r}\sigma_M = \frac{2(1-v-bv)}{(1-b)\alpha_M^{-1} + (b+1)(1-2v)}K_{Ie}\,. \quad (1.31)$$

For the comparison, the experimental and numerical modeling are also studied. Maletta et al. numerically modeled the case through FEA and made an experiment using single edge crack NiTi specimen [28]. It is observed that both methods show agreements in terms of crack distribution and transformation region as shown on the following Figure 1.10.

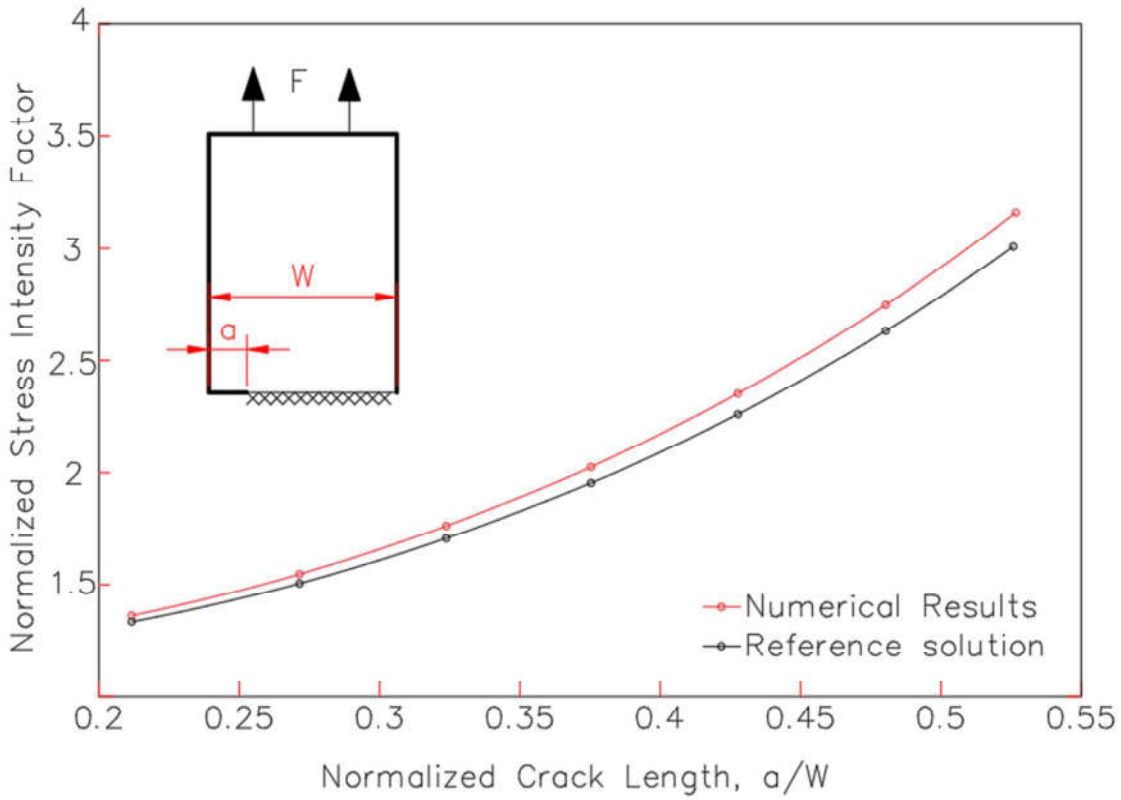

Figure 1.10. Effect of normalized crack length on normalized stress intensity factor.

As explained above, in numerous SMA studies, it is shown that there is a close correlation between crack tip stress distribution and asymptomatic equations of LEFM. Although the stress intensity factor B is replaced with K_e (effective stress intensity factor) in conjunction with the martensitic transformation. Based on this analogy, Ramberg-Osgood equation is studied to represent stress strain behavior and the size of martensitic transformation region is calculated by asymptotic equations HRR fields [29]. In HRR fields, named after Hutchinson, Rice, Rosenberg (1968), it is proposed that, a non-linear stress relation by using Ramberg-Osgood equation found as follows

$$\frac{\epsilon}{\epsilon_y} = \frac{\sigma}{\sigma_y} + \propto \left(\frac{\sigma}{\sigma_y}\right)^n, \tag{1.32}$$

where n is the hardening coefficient and α is calculated from yield off-set [30]. The corresponding stress function is expressed as:

$$\bar{\sigma}_{ij}(r,\theta) = \left(\frac{\bar{J}}{\alpha I_n \bar{r}}\right)^{\frac{1}{1+n}} \tilde{\sigma}_{ij}(\theta) \tag{1.33}$$

in which the singularity of the stress depends on *r* as follows:

$$\theta \sim r^{\frac{-1}{1+n}}. \tag{1.34}$$

Noting that in LEFM, $\theta \sim r^{\frac{-1}{1+n}}$, which results in a formulation modified due to plastic deformation. In the works of Anlaş et al. [30] this analogy between SMAs and plastic materials is employed to capture the primary features of SMA materials containing Mode I configuration cracks.

1.6.2. Full Field Finite Element Based Models

In the literature, full field FEA models are studied by Anlaş et al. [30] by imposing edge crack simulations to identify the effecting factors of stress and strain distributions. A 2-D plane stress model is designed and upper half of the crack is simulated since there is symmetry. The mesh is composed of second order, reduced integration, eight-node plane stress elements (CPS8R). In the Figure 1.11, the σ_{yy} distribution ahead of an SMA system modeled by FEA based ZM model [31] and HRR based approximation is compared with conventional LEFM.

The comparison is started with fitting Ramberg-Osgood equation to the ABAQUS stress-strain diagram. The specimen is loaded with decreasing loads from material system 1 to 3 and for different material systems KI, amplitude of the stress function in HRR solution and κ are calculated by J-Contour Integral in the ABAQUS. In order to observe results related to n parameter in Ramberg-Osgood equation, opening stress distributions around crack tip are plotted and especially in the transformation region consistency between LEFM and FEA obtained.

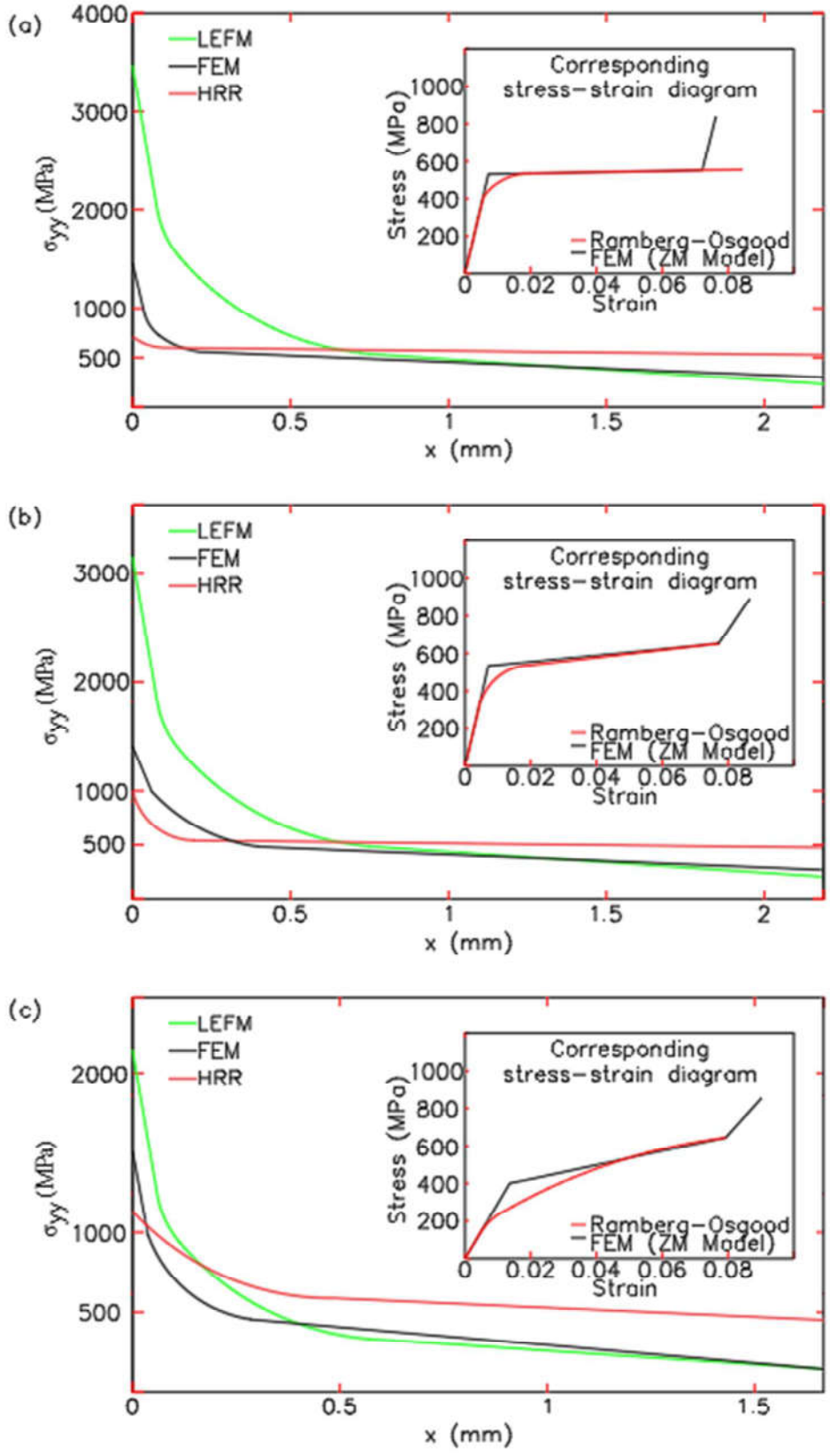

Figure 1.11. σ_{yy} distribution and corresponding stress strain diagram for three material systems.

As can be seen, FEA results compared to HRR and LEFM, results in σ_{yy} stress values higher than σ_{MS} in the transformation region. It should be emphasized that HRR results show better agreement with the FEA, since the LEFM method approach increases significantly with the square root singularity neglecting the transformation at the tip. Based on these results, it can be concluded that in the transformation region, the HRR equation is dominant and it is named as J dominant. In the austenitic region, LEFM method defines crack tip fields and so K dominant zone is defined. However, the zone boundaries are yet to be defined.

1.6.3. The Constitutive Behavior

There are multiple number of material parameters that effects the crack behavior of the model in the fracture. In addition to that, when the multiple phases are introduced in the SMA fracture mechanism, there is a need to build a model that can vary all the parameters for different zones around the crack tip. Therefore, the various state variables are proposed in the literature to define the phase transformation, mvf and energy dissipation during phase change as an example.

In the ABAQUS software, Auricchio et al. [32, 33] model is implemented to study super elastic behavior. Auricchio model is optimal for this thesis since the isothermal structure is defined by tonsorial variables and there the prediction of martensite reorientation is evaluated accurately. Another advantage of Auricchio Model is very few numbers of material properties are required and they are easily experimentally obtainable values.

Auricchio Model start with defining material properties in the different phase zones. The martensite fraction, ζ, is introduced in the formulation in order to evaluate the transformation zone properties as follows [34]:

$$E = E_A + \zeta(E_M + E_A) \tag{1.35}$$

$$v = v_A + \zeta\,(v_M + v_A). \tag{1.36}$$

As it can also be evaluated from the above formulation, the martensitic zone is following martensitic material properties as the ζ is 1 and for austenitic region the austenitic

material properties are obtained as the ζ is 0. The elastic deformation rules are followed for these two one-phase zones.

The above explained material properties are used to define uniaxial super elastic material phenomenon. The total strain increment, Δε, is obtained by summation of the elastic strain increment and the transformation strain increment. Transformation strain increment is calculated as follows:

$$\Delta\varepsilon^{tr} = \Delta\zeta \frac{G^{tr}}{\partial\sigma}. \tag{1.37}$$

The Drucker-Prager formulation is introduced to parametrize the transformation flow potential, G^{tr}, which is

$$G^{tr} = q - p \tan\psi, \tag{1.38}$$

where p is the equivalent pressure stress and the q is the Mises equivalent stress. The transformation surface also follows the Drucker-Prager form as below:

$$F^{tr} = q - p \tan\beta, \tag{1.39}$$

where β and ψ are angles obtained from transformation stress. The values for the above-mentioned material properties except tabulated in the Table 2.1 are adopted from literature reviews [35,36].

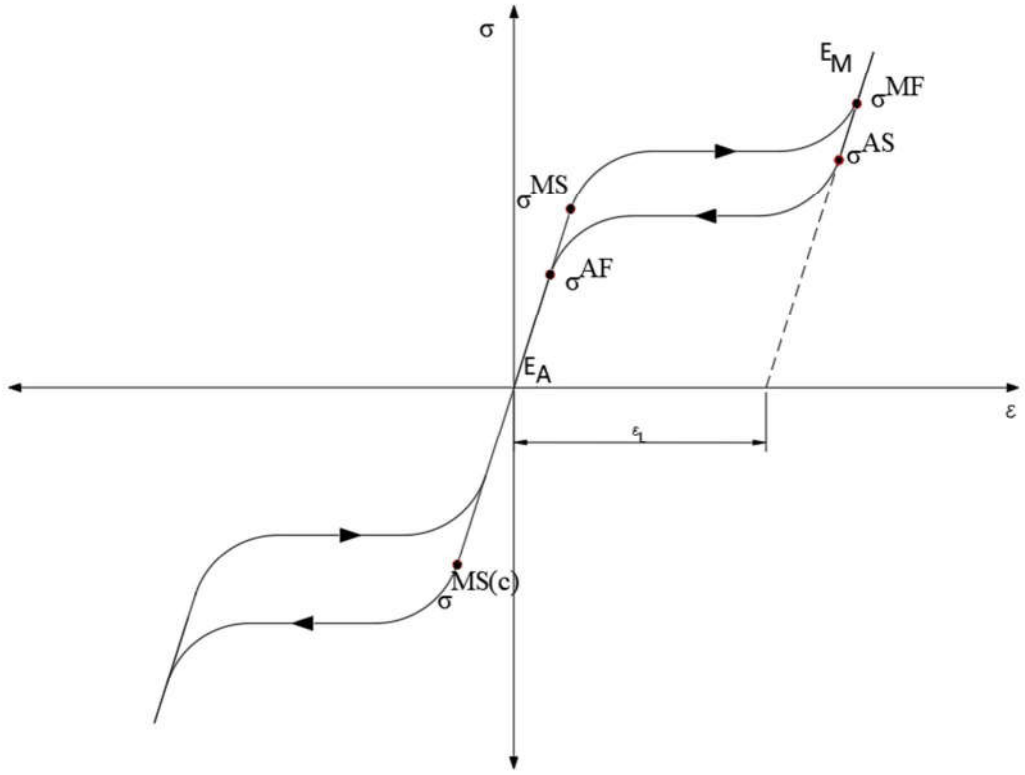

Figure 1.12. Superelastic behavior of SMA under loading and unloading conditions.

2. PROBLEM DESCRIPTION AND METHODOLOGY

2.1. Inclined Crack Configuration and Material Properties

The inclined crack configurations are implemented using the same material constants and the meshing framework. The simulation is designed as per below 2D model. Every simulation is run for α equals 0°, 10°, 20° and 30°.

Same simulation model with additional material properties specified is designed to show the effect of the super elasticity on crack propagation. The following Table 2.1 is prepared in order to summarize the super elasticity material property changes between simulations. The constant material property is Young's Modulus for martensite E = 35 GPa.

Table 2.1. Material Properties for Each Simulation.

	Young's Modulus [GPa]	Transformation Strain	Start of Transformation (Loading) [MPa]	End of Transformation (Loading) [MPa]	Start of Transformation in Compression (Loading) [MPa]
Sim 1	35	0.06	200	205	200
Sim 2	35	0.1	200	205	200
Sim 3	35	0.1	200	250	200
Sim 4	35	0.1	150	200	150
Sim 5	35	0.06	150	200	150
Sim 6	35	0.04	150	200	150
Sim 7	35	0.1	200	300	200
Sim 8	35	0.04	200	205	200
Sim 9	35	0.1	300	305	300
Sim 10	35	0.1	400	405	400

The size of the specimen is 100 mm width and 200 mm height. The crack plane length is 25 mm and kept constant for all simulations. Therefore, a/w ratio is 0.25. The square shaped mesh size around the crack tip is set as 0.01 mm for a specific region which is shown in the Figure 2.1.b and 2.1.c.

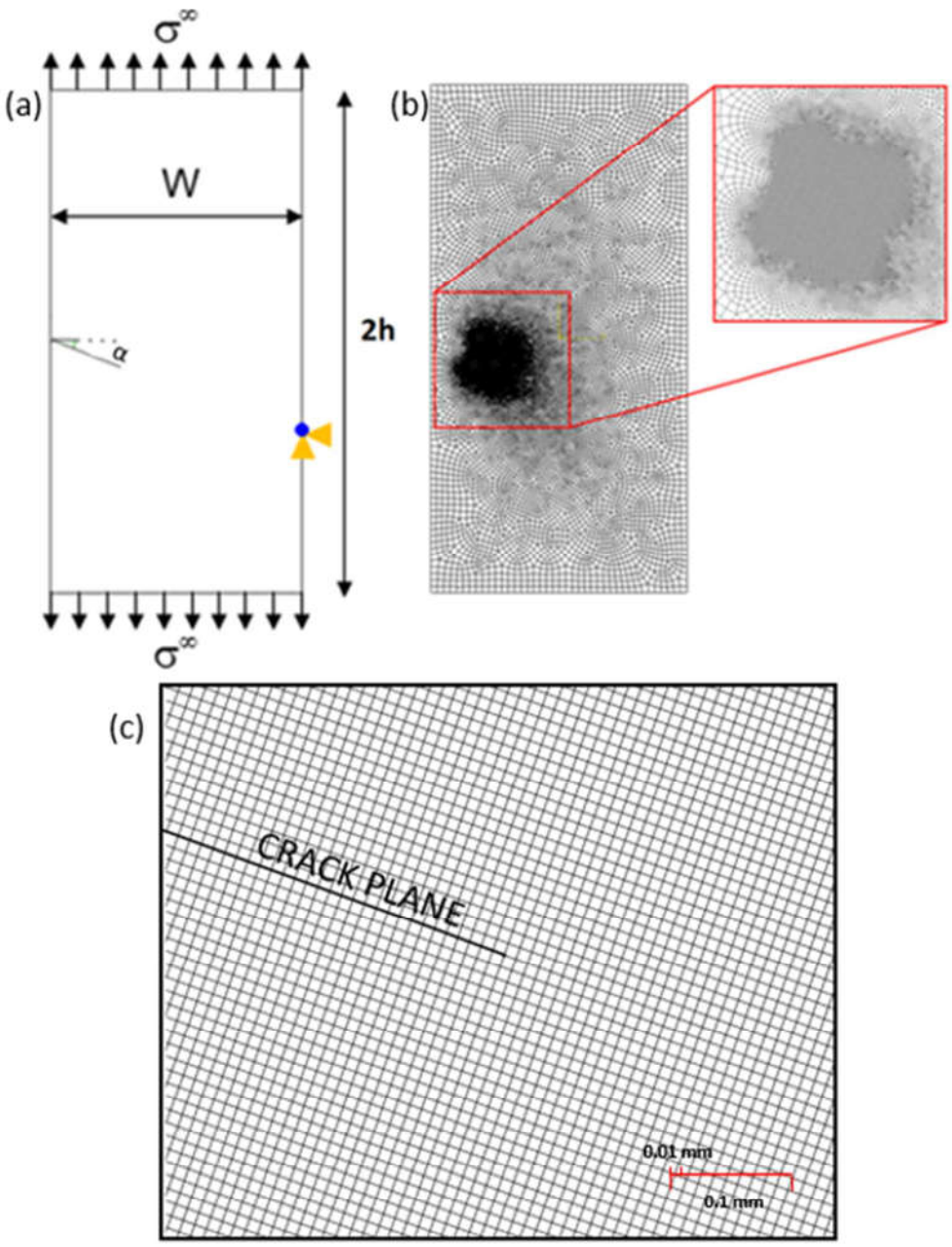

Figure 2.1. (a) Schematic representation of edge cracked plate under Mixed Mode loading.
(b) CPS8 meshes around crack tip and crack plane for Mixed Mode I loading.
(c) Square meshes around crack tip.

2.2. Data Collection for Crack Evaluation

The materials that are described in the Table 2.1, are considered for further crack evaluation optimizations. The below described methodology is followed for collecting data from ABAQUS software.

Primarily, 11 parallel node paths are defined on ABAQUS software for each crack angle. Each path consists of 11 consecutive nodes. The path number increases towards upwards direction and the first node on the Path 6 corresponds to crack tip, therefore it may be excluded on the following fitting calculations if there are non-singularities. The singularity related studies are studied by Özerim[37]. The 0° case nodal placements are represented in below Figure 2.2.

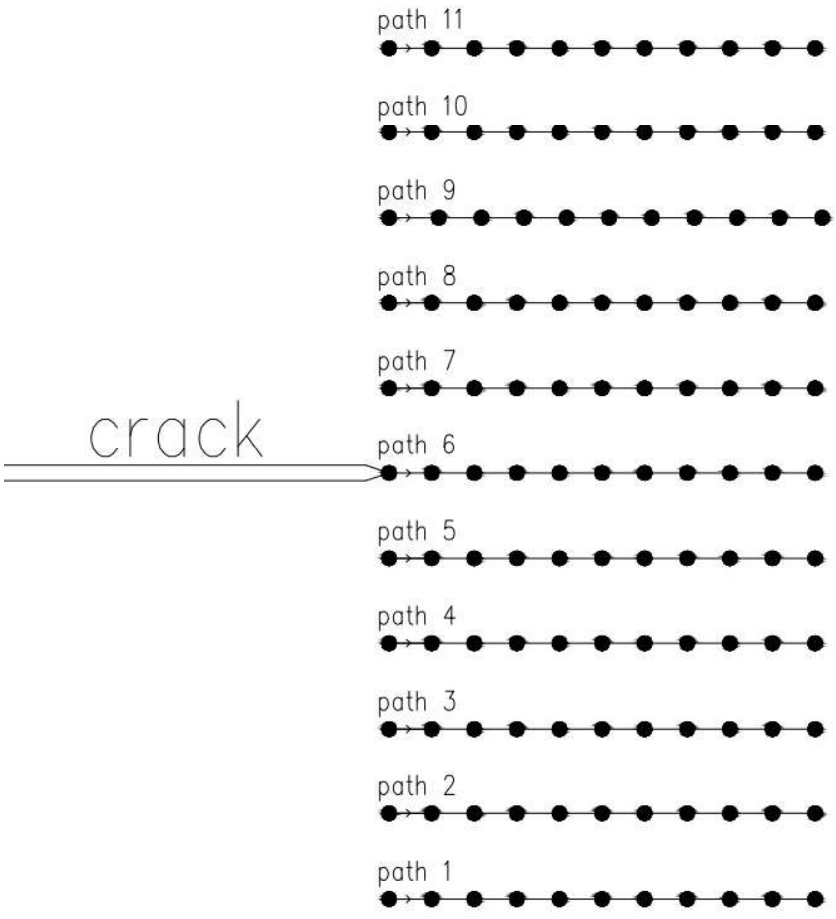

Figure 2.2. 0° simulation nodal placements.

Using predefined paths, x coordinate, y coordinate, stress at x direction (σ_{xx}), stress at xy direction (σ_{xy}), stress at y direction (σ_{yy}) and martensite volume fraction for each node are extracted. Afterwards, the derived parameters, such as distance of node to crack tip in x and y direction and so polar coordinates of the node at crack tip originated reference system is computed as shown in Figure 2.3. As the crack reference system does not coincide with the global reference system, for 10° , 20° and 30° cases, additional stress transformations were done to obtain stress values with respect to the coordinate system that is parallel to the crack plane.

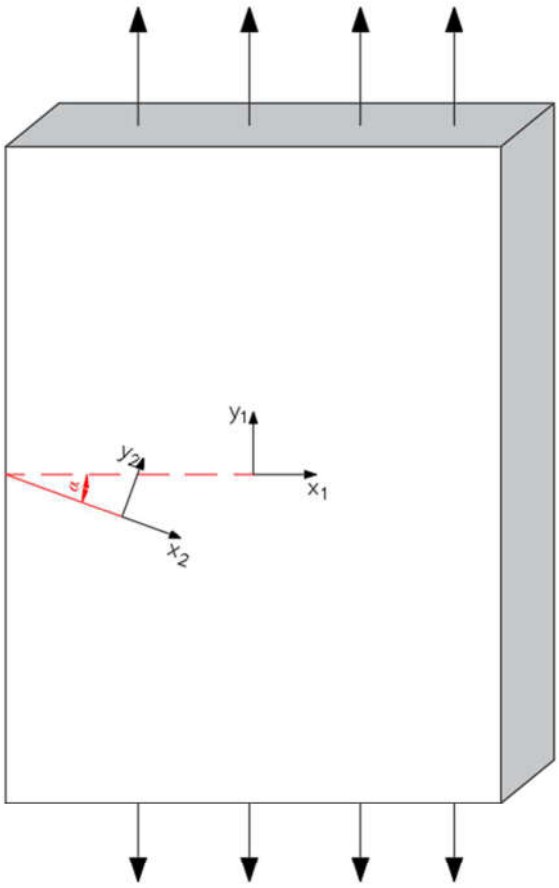

Figure 2.3. Global (1) and crack tip oriented (2) reference system.

Additionally, as the literature in fracture mechanics mainly focuses on the polar coordinates for the derivation of stresses, the stresses that are calculated by ABAQUS, are optimized to a reference system that is parallel to the crack plane in MATLAB and converted to polar cylindrical coordinates by the below matrix mapping:

$$\begin{bmatrix} \sigma_{rr} & \sigma_{r\theta} & \sigma_{rz} \\ \sigma_{\theta r} & \sigma_{\theta\theta} & \sigma_{\theta z} \\ \sigma_{zr} & \sigma_{z\theta} & \sigma_{zz} \end{bmatrix} = \begin{bmatrix} cos\theta & sin\theta & 0 \\ -sin\theta & cos\theta & 0 \\ 0 & 0 & 1 \end{bmatrix} \begin{bmatrix} \sigma_{xx} & \sigma_{xy} & \sigma_{xz} \\ \sigma_{yx} & \sigma_{yy} & \sigma_{yz} \\ \sigma_{zx} & \sigma_{zy} & \sigma_{zz} \end{bmatrix} \begin{bmatrix} cos\theta & -sin\theta & 0 \\ sin\theta & cos\theta & 0 \\ 0 & 0 & 1 \end{bmatrix}, \quad (2.1)$$

which can be simplified to below equations:

$$\sigma_{rr} = \sigma_{xx}cos^2\theta + \sigma_{yy}sin^2\theta + \sigma_{xy}\sin(2\theta) \quad (2.2)$$

$$\sigma_{\theta\theta} = \sigma_{xx}sin^2\theta + \sigma_{yy}cos^2\theta - \sigma_{xy}\sin(2\theta) \quad (2.3)$$

$$\sigma_{r\theta} = sin\theta cos\theta\left(\sigma_{yy} - \sigma_{xx}\right) + \sigma_{xy}\cos(2\theta). \quad (2.4)$$

2.3. Non-Linear Least Squares Fit Regression

As the ABAQUS data is not continuous and only valid for the node points around the crack tip, a continuous model is needed in order to process the data more efficiently. It is known that due to stress induced martensitic transformation around the crack, the parameters extracted from ABAQUS are not linear and rely on multiple parameters. Therefore, a statistical model, nonlinear regression is proposed to fit ABAQUS data. The nonlinear regression methodology is basically approximating a nonlinear function from linear functions by doing successive iterations [38] as follows:

$$y_t = f(x_t, a_k) + e_t \qquad t = 1,2,3,\dots,n\,, \quad (2.5)$$

where $f(x_t, \theta)$ is a function of x_t, the inputs, a, vector of k number of unknown values and e_t, the error parameter [39]. The primary step for the model is to relate the y_t (dependent data) to the x_t data on the significant part of the model by a linear or polynomial fit. Afterwards, the estimation of the predefined fit into the more accurate fit may be done by various ways [40].

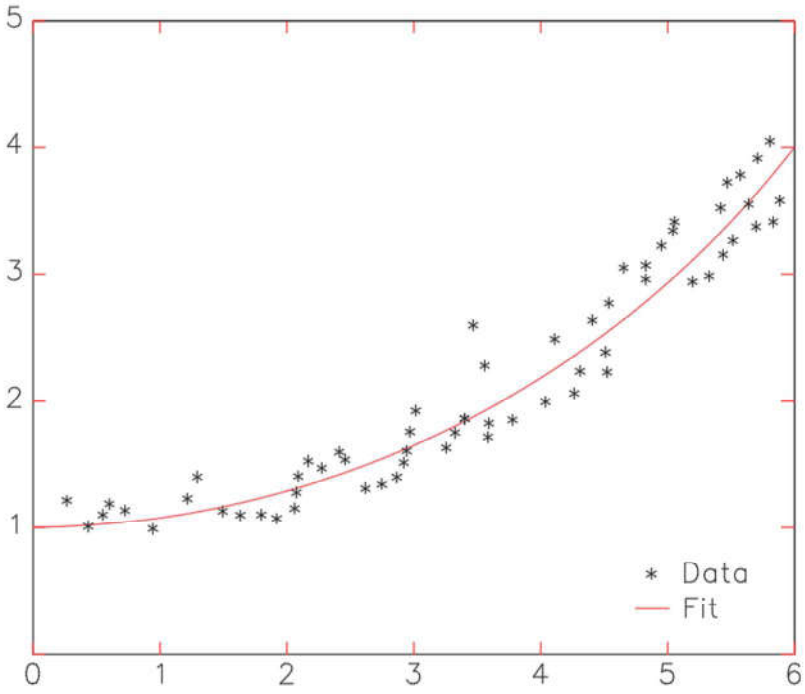

Figure 2.4. Fitting pointwise data to exponential curve by lsqnonlin.

Most commonly, sum of the least squares method is used for optimization. This method refines the data by achieving the minimum of the values between y_t (observed data) and y_{fit} by successive iterations as follows

$$SS = \sum [(y_t - f(x_t, a_k))^2], \tag{2.6}$$

where SS is the sum of the squares of the residuals. According to the theorem the ideal fit corresponds to the S=0 value. To solve this fit problem, Taylor Series expansions are used in order to approximate [41]. High order case example as follows

$$y_t - f(x_t)_j = \frac{\partial f(x_t)_j}{\partial a_0}\Delta a_0 + \frac{\partial f(x_t)_j}{\partial a_1}\Delta a_1 + \cdots + e_i\,, \tag{2.7}$$

which is in matrix form,

$$\{D\} = [Z_j]\{\Delta A\} + \{E\}, \tag{2.8}$$

where Z is the matrix of partial derivatives evaluated at the t[th] data point. D is the vector of the differences; A is the vector of the differences in the parameter values. These steps are followed by solving above matrix equation for the $\{\Delta A\}$:

$$a_{k,j+1} = a_{k,j} + \Delta a_k \,. \tag{2.9}$$

And the procedure stops when the increment is below the predefined stop value ε which is generally accepted as converging limit as shown below equation:

$$\varepsilon > \left| \frac{a_{k,j+1} - a_{k,j}}{a_{k,j+1}} \right|. \tag{2.10}$$

The method requires initiation point for every parameter which are generally predicted in least square fit applications. The first guess value is iterated many times until it is close enough to the curve. The distance between fit curve and original curve is generally defined primarily depending on the need of the application. This optimization may be done by few methods. The most common used optimizations are steepest decent method, Gauss-Newton method and Levenberg-Marquardt method [42, 44].

The steepest decent method is effective especially for the initial iterations. By moving predefined step length, the decent and therefore slope is computed repetitively and minimum point of the curve is aimed. With increasing number of iterations, sharp turns are obtained and accuracy of the fit curve is decreasing [42,43].

The Gauss-Newton method tries to approximate the curve, with the help of the initial point, to an ellipsoid. Afterwards, by using known parameters, the methodology predicts minimum for the ellipsoid and from that point new ellipsoid is approximated on the curve repeatedly [45,44].

Especially, in nonlinear curves, it is hard to fit ellipsoidal shape and accuracy of the first guess has crucial importance. Therefore, especially in initial iterations, the Gauss-Newton method is more likely to be unsuccessful.

The Levenberg-Marquardt method can be defined as the combination of the previous two methods. The steepest decent model is used primarily as it is more accurate in the primary steps until the point that the sum of least squares is negligibly small. At that point, the method changes to Gauss-Newton model as it is more accurate in the progressive iterations [42, 46,47,48].

Since more iterations cause more accurate solutions in general, usage of the computational programs is very important for this regression. In this thesis for such purpose, the MATLAB software non-linear least squares solver function, "lsqnonlin", is chosen. Instead of calculating the sum of squares as in traditional methods, "lsqnonlin" works with user defined function for computation [40].

In order to operate the "lsqnonlin" function for MTS Criterion, a user-defined error function is proposed. The function computes a vector of differences between input stress values and predicted values. As MATLAB software require predefined criterions for termination, the max iterations are limited to 65000 with function and step tolerance are 10^{-6}.

The stress function and error function for the σ_{rr}^{fit} is proposed as follows:

$$\sigma_{rr}^{fit} = k_{eq}\,[\sin(m\theta)\cos(n\theta) + \sin(v\theta) + \cos(t\theta)]\frac{1}{\sqrt{2\pi r}} \tag{2.11}$$

$$f_{Err} = \sigma_{rr} - \sigma_{rr}^{fit} \tag{2.12}$$

as m, n, v and t are the coefficients that are defined to parametrize the function also with the coefficient k_{eq}. The numerical values for k_{eq}, m, n, v and t are predicted as 30, 1, 1, 2 and 1, respectively.

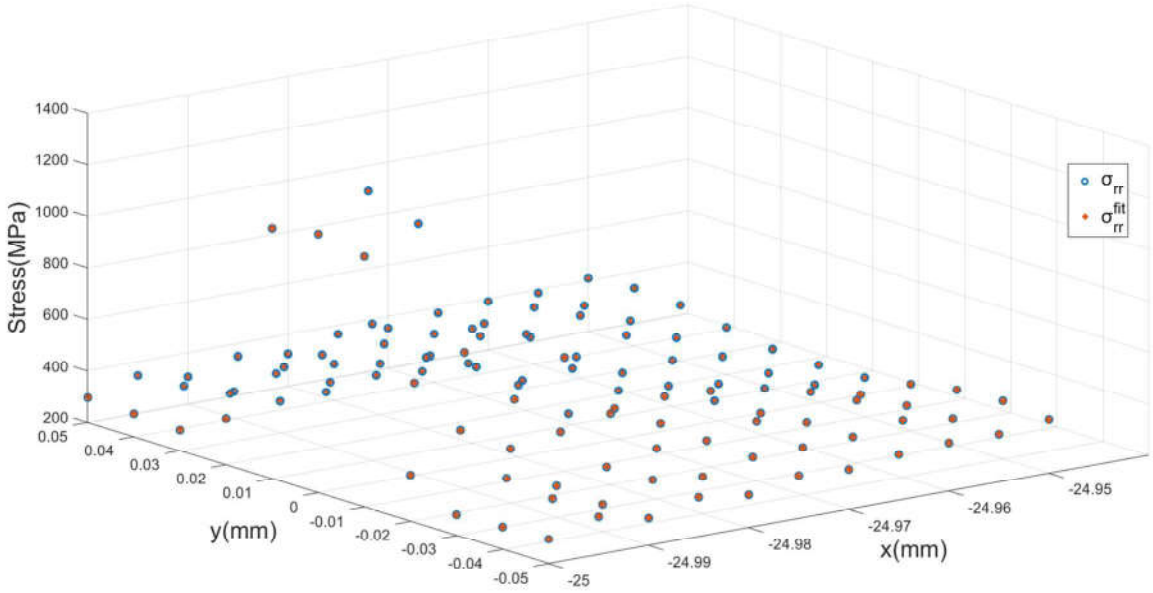

Figure 2.5. ABAQUS nodal data – MATLAB fit equivalent for σ_{rr}.

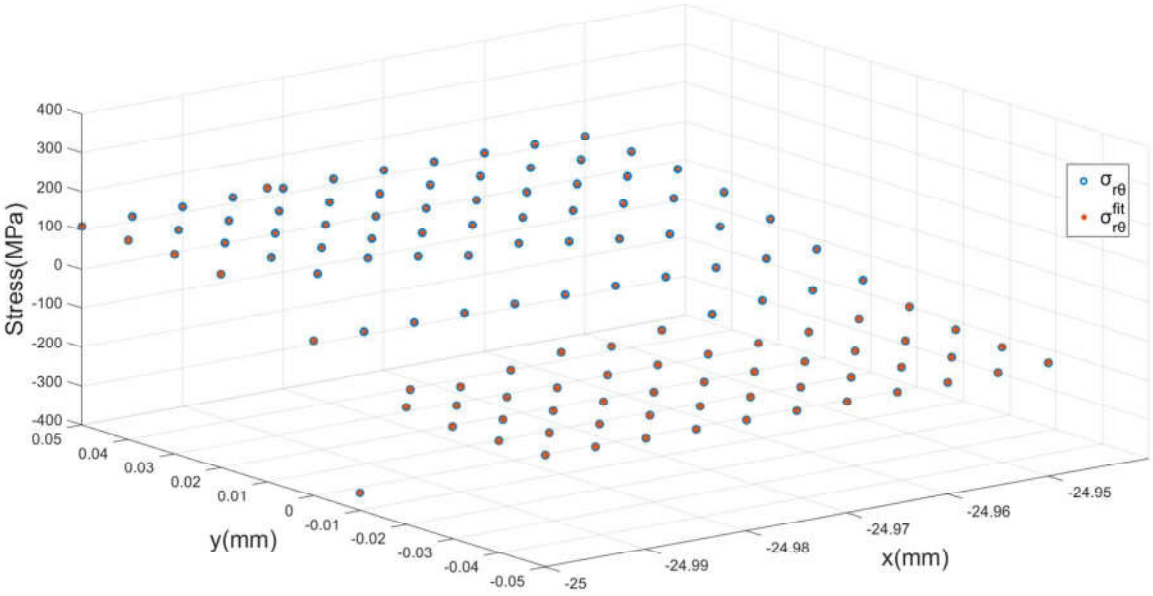

Figure 2.6. ABAQUS nodal data – MATLAB fit equivalent for $\sigma_{r\theta}$.

After defining the error function, the “lsqnonlin” function returns a series of output that iterates the error function until the change in the residual is smaller than the specified tolerance. The results are calculated for every nodal value and verified by comparing to ABAQUS values as in the Figure 2.5, 2.6 and 2.7.

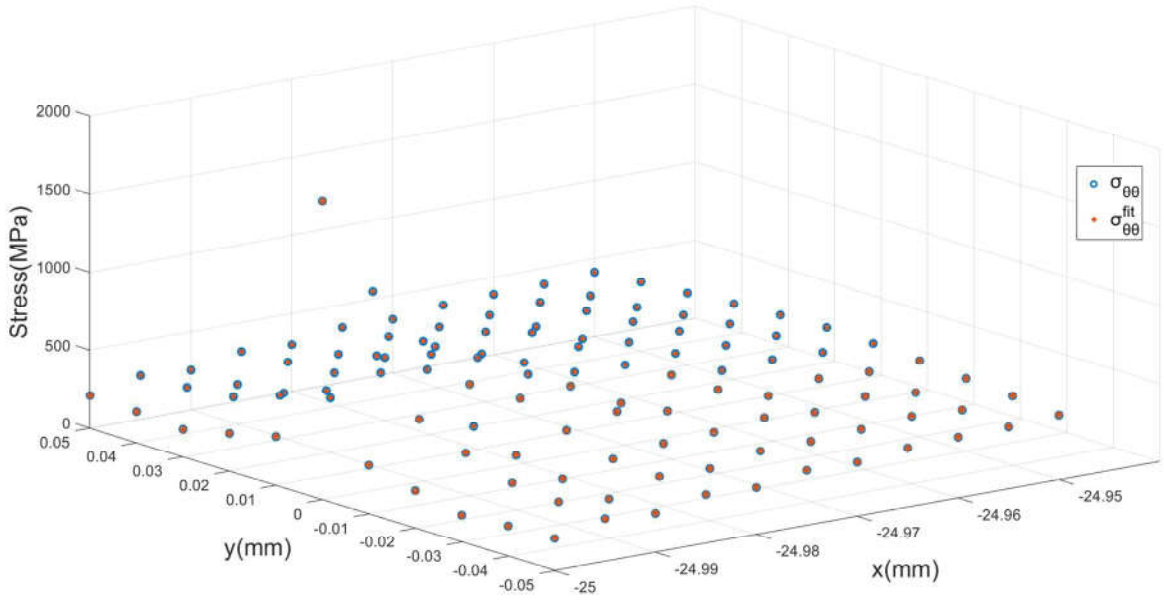

Figure 2.7. ABAQUS nodal data – MATLAB fit equivalent for $\sigma_{\theta\theta}$.

For the Sim 4, 0° case stress values from ABAQUS software (σ_{rr}, $\sigma_{r\theta}$, $\sigma_{\theta\theta}$) and MATLAB fit stress values are plotted vs Cartesian coordinates as can be seen from Figure 2.5, 2.6 and 2.7 respectively. The blue data (circle) represents the data taken from ABAQUS and red data (star) shows the MATLAB fit. The errors in the fit are negligibly low that in the graph values almost coincide.

3. CRACK INITIATION CRITERIONS AND IMPLEMENTATION TO THE SMAs

3.1. MTS Criterion

In 1963, Erdogan and Sih [49] proposed the MTS Criterion. Their initiation point to predict the behavior of the crack is finding the maximum tension as crack will start perpendicular to it. Additionally, MTS criterion proposes that crack propagates when the maximum tangential stress coincides with the crack growth direction and reaches the critical value [49,50,51], so it is defined as

$$\frac{d\sigma_{\theta\theta}}{d\theta} = 0, \qquad \frac{\partial^2 \sigma_{\theta\theta}}{\partial \theta^2} < 0\,. \tag{3.1}$$

In this thesis, the MTS criterion is studied by using the stresses in Cartesian coordinates from the ABAQUS model instead of analytical calculations. The stresses in Cartesian coordinates are transferred to polar coordinates by additional formulation as explained in the previous chapter by MATLAB software. In order to obtain $\sigma_{\theta\theta}$, the Equation (3.2), (3.3) and (3.4) are implemented in "lsqnonlin" code:

$$\sigma_{rr}^{fit} = k_{eq1}[\sin(m_1\theta)\cos(n_1\theta) + \sin(v_1\theta) + \cos(t_1\theta)]\frac{1}{\sqrt{2\pi r}} \tag{3.2}$$

$$\sigma_{r\theta}^{fit} = k_{eq2}[\sin(m_2\theta)\cos(n_2\theta) + \sin(v_2\theta) + \cos(t_2\theta)]\frac{1}{\sqrt{2\pi r}} \tag{3.3}$$

$$\sigma_{\theta\theta}^{fit} = k_{eq3}[\sin(m_3\theta)\cos(n_3\theta) + \sin(v_3\theta) + \cos(t_3\theta)]\frac{1}{\sqrt{2\pi r}}. \tag{3.4}$$

3.2. S Criterion

G.C. Sih proposed that crack will initiate in a radial direction along which the strain energy density is minimum[52,53]. The strain energy density is defined in Equation (3.6) and this integral represents the area under the stress strain curve of a specimen. This area is also related to the work done by load for a specimen under tensile loading. Therefore, it can

be used as a measure to calculate material's ability to absorb energy up to fracture which is toughness [54]. Since the $S_{cr}(\theta)$, critical strain energy density for crack initiation, is not related to geometry of crack or loading geometry, it makes S Criterion suitable for this evaluation. For this purpose, the crack initiation criterion is defined as

$$\frac{\partial S(\vartheta)}{\partial \theta} = 0, \quad \frac{\partial^2 S(\vartheta)}{\partial \theta^2} > 0 \tag{3.5}$$

where S is quadratic strain energy density function derived from above defined U, strain energy density function:

$$U = \frac{dU_s}{dV} = \int \sigma_{ij} d\varepsilon_{ij} \quad (i,j = 1,2,3)\,. \tag{3.6}$$

The criterion is adopted to thesis by several steps on ABAQUS and MATLAB software. Firstly, the strain energy density around crack tip on integration points are extracted from ABAQUS. By using the coordinates of integration points with respect to crack tip, the angle between the integration point and crack plane, θ and distance to the crack tip, r, are calculated.

Secondly, the non-continuous data around the crack tip shall be made continuous in order to calculate the derivative and find the minimum point of the S(θ). Similarly, to the MTS criterion, the lsqnonlin function in the MATLAB is used for such purpose. By using the user defined error function, the fit is obtained. However, it should be underlined that the fit function does not have any physical meaning since nodal points are fitted as a user defined trigonometric function and coefficients only.

3.3. T Criterion

T Criterion in fracture mechanics is used to define maximum dilatational strain energy density criterion. Previously defined, S and MTS criterions are more accurate to define brittle fracture however T Criterion is more accurate to define ductile fracture. Theocaris [55, 56, 57] defined two strain energy parameters which are the dilatational (U_V)

and distortional strain energy density (U_D). The criterion defines crack initiation direction as the maximum dilatational strain energy density direction on the contour of constant distortional strain energy around the crack tip as follows

$$\frac{\partial U_v}{\partial \theta} = 0, \qquad \frac{\partial^2 U_v}{\partial \theta^2} < 0\,. \tag{3.7}$$

With the aim of the implementing this criterion on this thesis, the dilatational strain energy is calculated by ABAQUS stress and transformation strain outputs. The hydrostatic strain is

$$\varepsilon_{hyd} = \begin{bmatrix} \frac{\varepsilon_{xx}+\varepsilon_{yy}+\varepsilon_{zz}}{3} & 0 & 0 \\ 0 & \frac{\varepsilon_{xx}+\varepsilon_{yy}+\varepsilon_{zz}}{3} & 0 \\ 0 & 0 & \frac{\varepsilon_{xx}+\varepsilon_{yy}+\varepsilon_{zz}}{3} \end{bmatrix} \tag{3.8}$$

and the dilatational strain energy is

$$U_V = \int \sigma_{ij}\, d\varepsilon_{ij}^{hyd} \qquad (i,j = 1,2,3) \tag{3.9}$$

and crack initiation criterion for the T Criterion is defined as

$$\frac{\partial^2 U_v}{\partial \theta^2} < 0 \tag{3.10}$$

and the distortional strain energy density is

$$U_D = S - U_V\,. \tag{3.11}$$

By knowing the distortional and dilatational strain energy densities, the previously defined “lsqnonlin” function is used in MATLAB to obtain continuous curve of ABAQUS

data. The same error function that is used as in the strain energy density criterion, is aimed to be defined by a function consisting of user defined trigonometric functions and coefficients.

3.4. Det Criterion

Papadapoulos [58,59,60] has simplified the strain energy density criterions by proving that the maximum value of Det(σ_{ij}) corresponds to the max value of dilatational strain energy density. Therefore, crack propagates with the same direction of the maximum stress tensor determinant value as follows

$$\frac{\partial Det(\sigma_{ij})}{\partial \theta} = 0, \qquad \frac{\partial^2 Det(\sigma_{ij})}{\partial \theta^2} < 0, \qquad \text{i,j} = 1,2,3\,. \tag{3.12}$$

The previously extracted ABAQUS stress values for MTS are used to calculate the Det(σ_{ij}) values to evaluate the criterion. After calculating the Det(σ_{ij}), the values are processed in the MATLAB by “lsqnonlin” function and a continuous curve is obtained for Det(σ_{ij}).

3.5. Ip Criterion

The Ip Criterion defines crack initiation in terms of stress invariants by using a similar approach to T-criterion. Ukadgaonker et. al.[61] used stress invariants to define the dilatational strain energy density criterion and therefore, T-Criterion is interpreted without calculating the strain energy densities. Therefore, T-criterion is evaluated in terms of stress values as shown below equation:

$$\frac{\partial U_v}{\partial \theta} = 0, \qquad \frac{\partial^2 U_v}{\partial \theta^2} < 0. \tag{3.13}$$

The dilatational strain energy Uv can be written as a function of Ip only where Ip is

$$I_p = I_1^2 - 2I_2 \tag{3.14}$$

where I_1 and I_2 are first and second stress invariants respectively. Therefore, instead of evaluating maximum dilatational strain energy density around crack tip, Ip can be used with the help of the Equation (3.14) as follows:

$$\frac{\partial I_p}{\partial \theta} = 0, \qquad \frac{\partial^2 I_p}{\partial \theta^2} < 0. \tag{3.15}$$

By the help of the above explained methodology, The ABAQUS extracted stress values are used to calculate stress invariants and therefore, the Ip factor. Afterwards, the pointwise calculated values on the nodes are implemented in MATLAB code to obtain a continuous fit and the maximum points are calculated.

4. RESULTS

4.1. Effect of Transformation Finish Stress

The Sim 2, Sim 3 and Sim 7 are studied in order to evaluate the effect of strain hardening effect since start of transformation under loading condition and transformation strain are equal but only transformation finish stress under loading condition is different. As martensite volume fraction is decreasing between the simulations respectively, the hardening effect similarly decreases.

The Figure 4.1, 4.2 and 4.3 represent the cases under different crack initiation criterions. Especially, the results may vanish similar results in the 0° and 10° cases. The general trend shows that deviation from the crack plane is increasing in the order of the Sim 2, Sim 3 and Sim 7. This can be explained by the strain hardening process as the toughness of the specimen is increasing especially behind the crack tip. This process is resulted with the deviation from the crack tip. Further interpretations are described in Discussion.

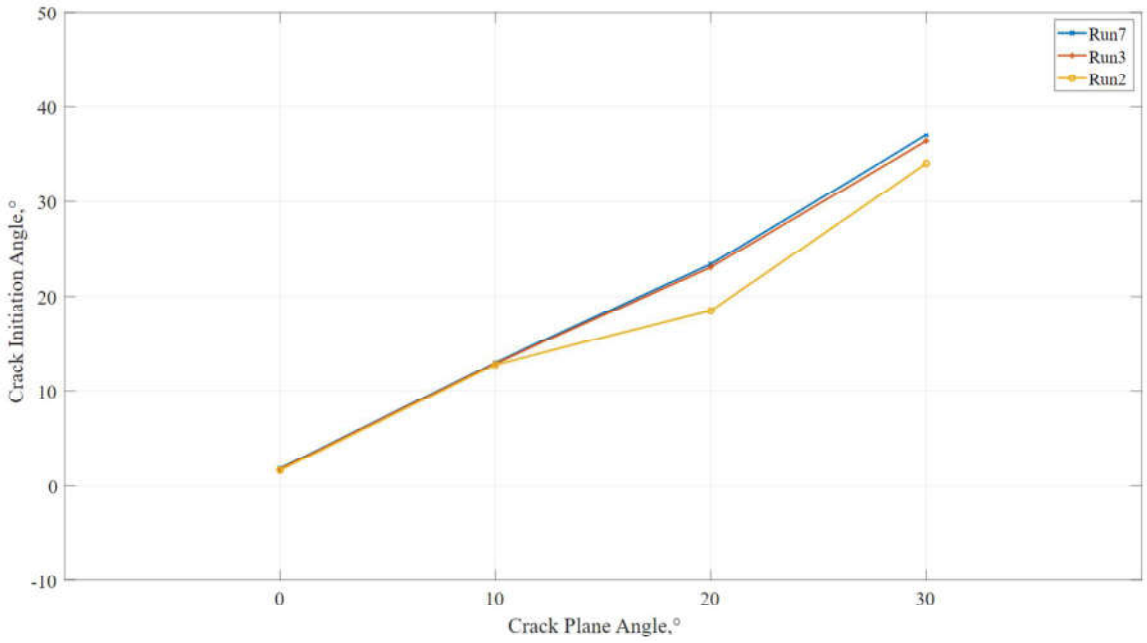

Figure 4.1. Crack initiation angles according to MTS criterion to evaluate effect of transformation finish stress.

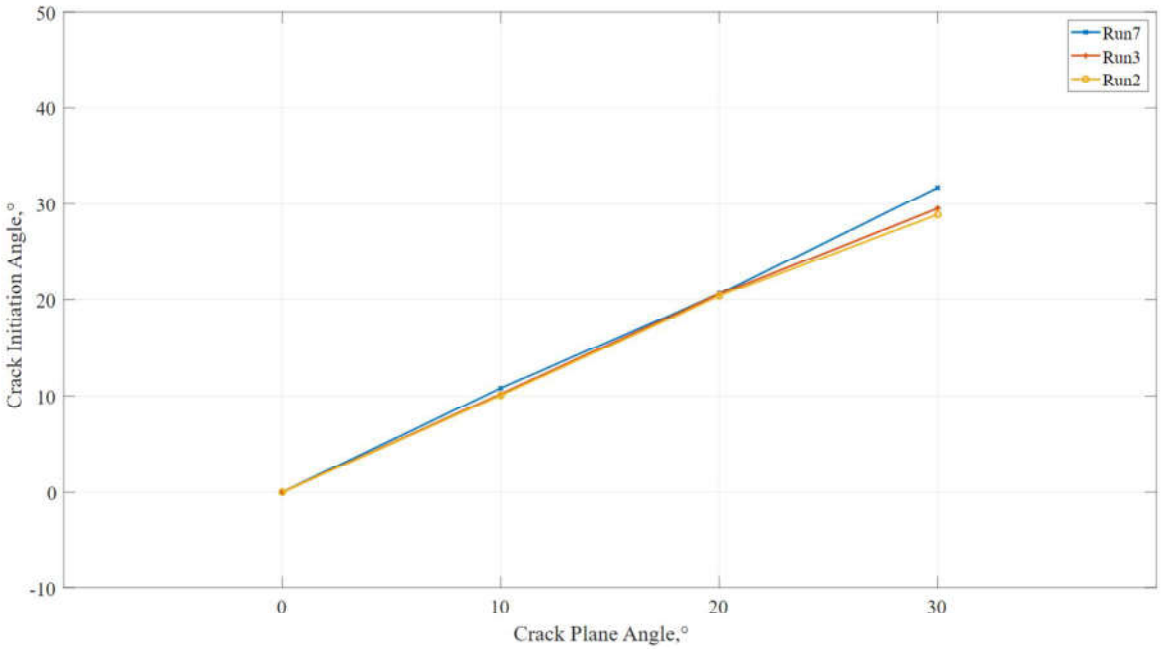

Figure 4.2. Crack initiation angles according to Det criterion to evaluate effect of transformation finish stress.

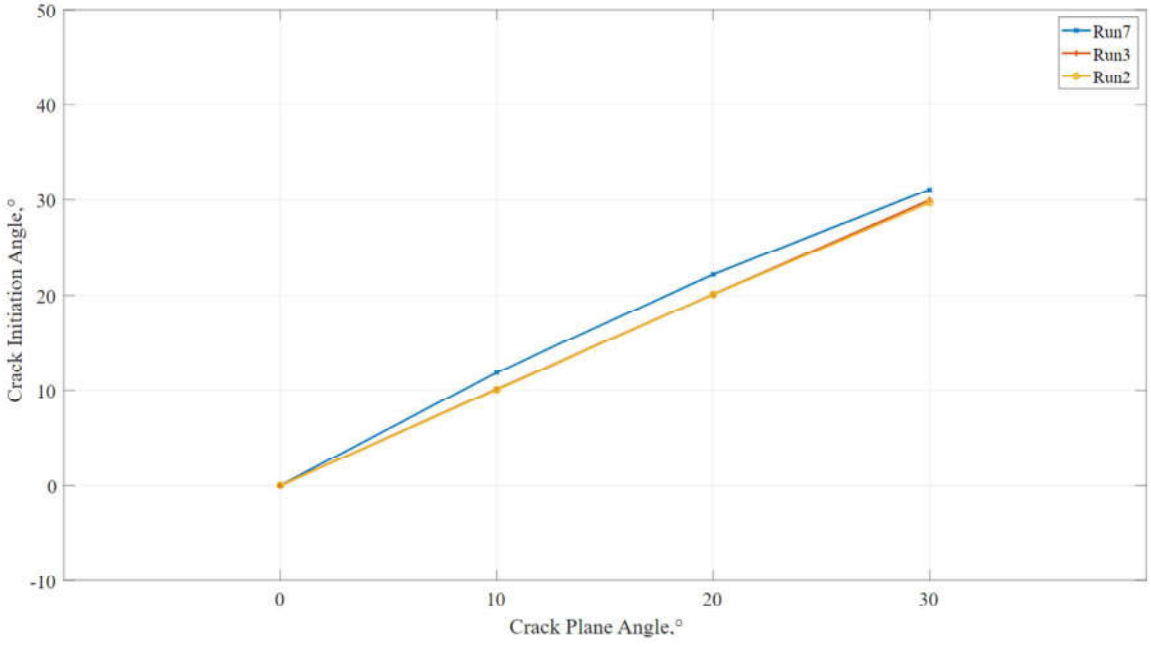

Figure 4.3. Crack initiation angles according to Ip criterion to evaluate effect of transformation finish stress.

4.2. Effect of Transformation Strain

The Sim 1, Sim 2 and Sim 8 are appropriate examples to see the effect of the transformation strain on the crack angle. The changing parameter is directly affecting the martensitic ratio under loading condition. For this simulation group, obtained results are given in Figure 4.4, 4.5 and 4.6.

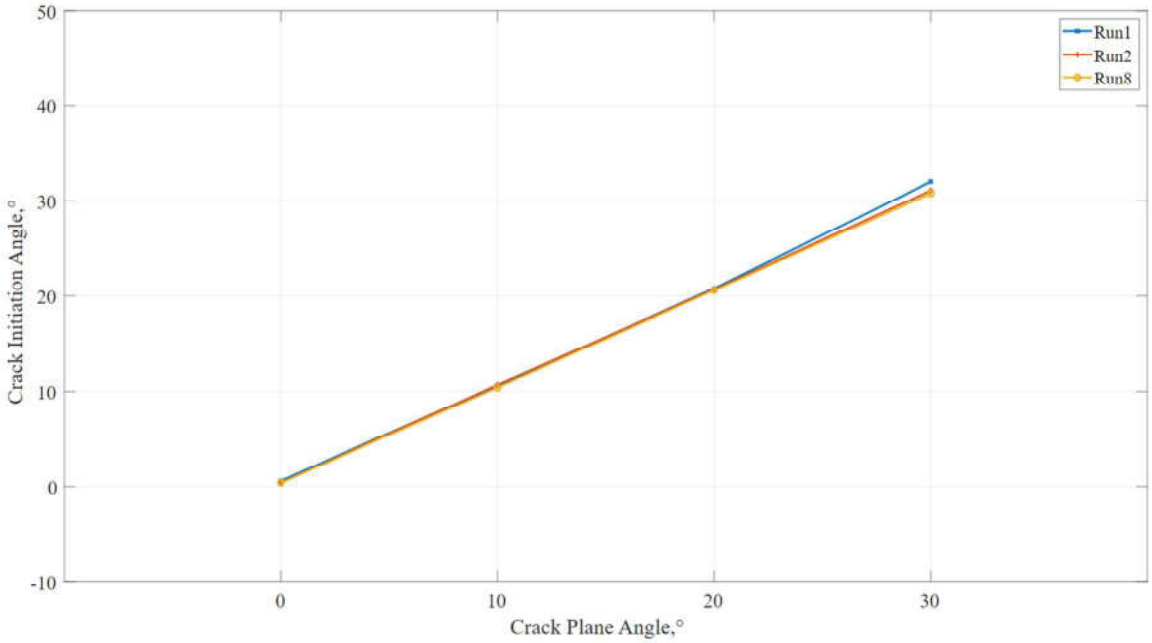

Figure 4.4. Crack initiation angles according to MTS criterion to evaluate effect of transformation strain.

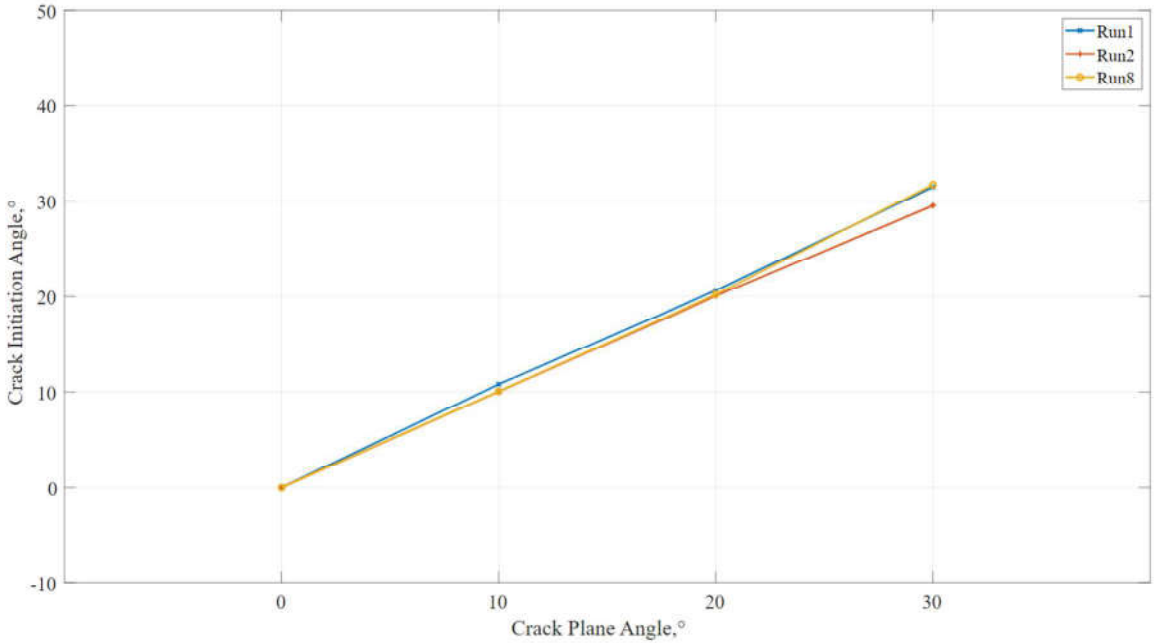

Figure 4.5. Crack initiation angles according to Det criterion to evaluate effect of transformation strain.

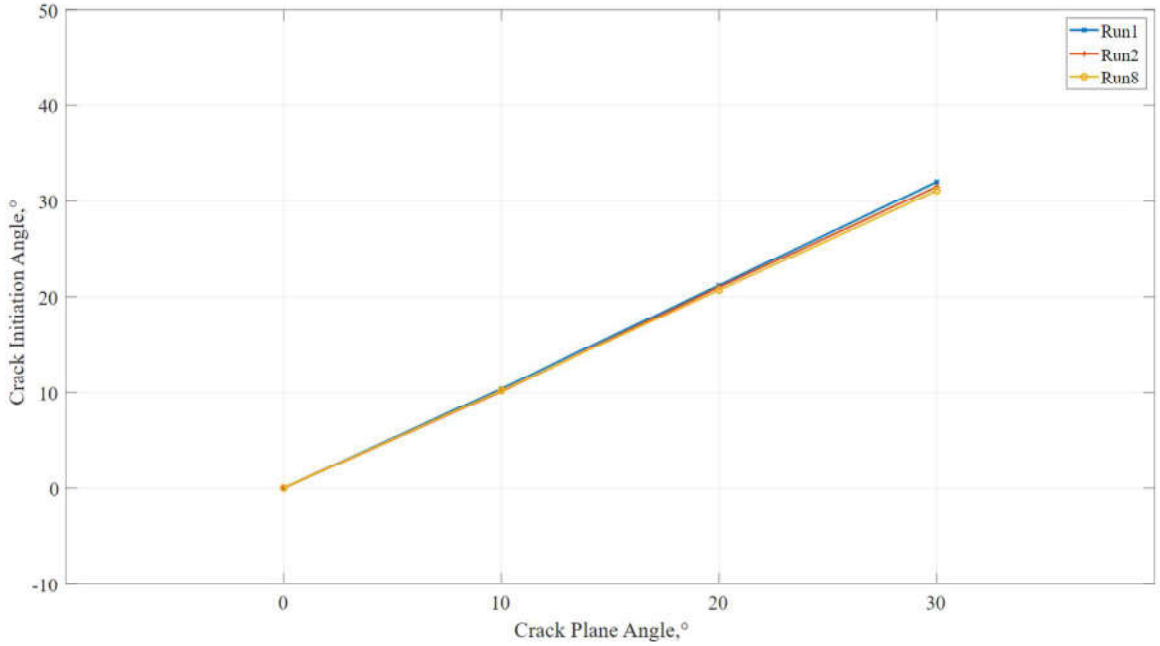

Figure 4.6. Crack initiation angles according to Ip criterion to evaluate effect of transformation strain.

4.3. Effect of Transformation Start Stress Levels

The Sim 2, Sim 9 and Sim 10 material properties are same in terms of transformation strain and there is difference between transformation start and end stresses. Therefore, the effect of the higher martensitic transformation stresses is studied between simulations. The results are shown in the Figure 4.7, 4.8 and 4.9.

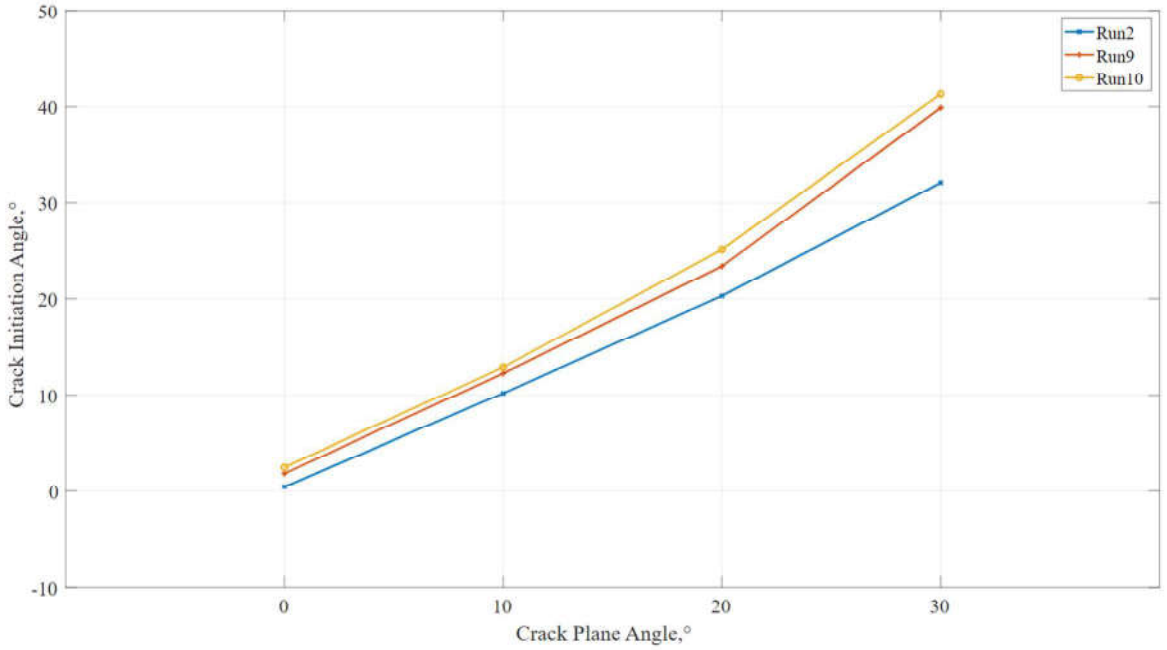

Figure 4.7. Crack initiation angles according to MTS criterion to evaluate effect of transformation start stress levels.

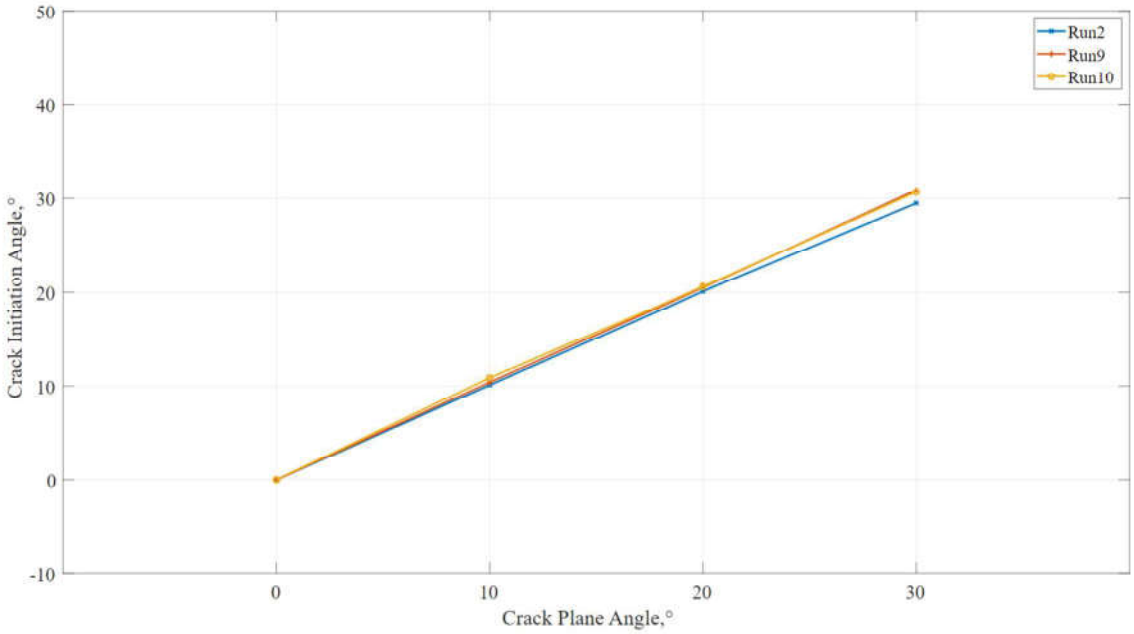

Figure 4.8. Crack initiation angles according to Det criterion to evaluate effect of transformation start stress levels.

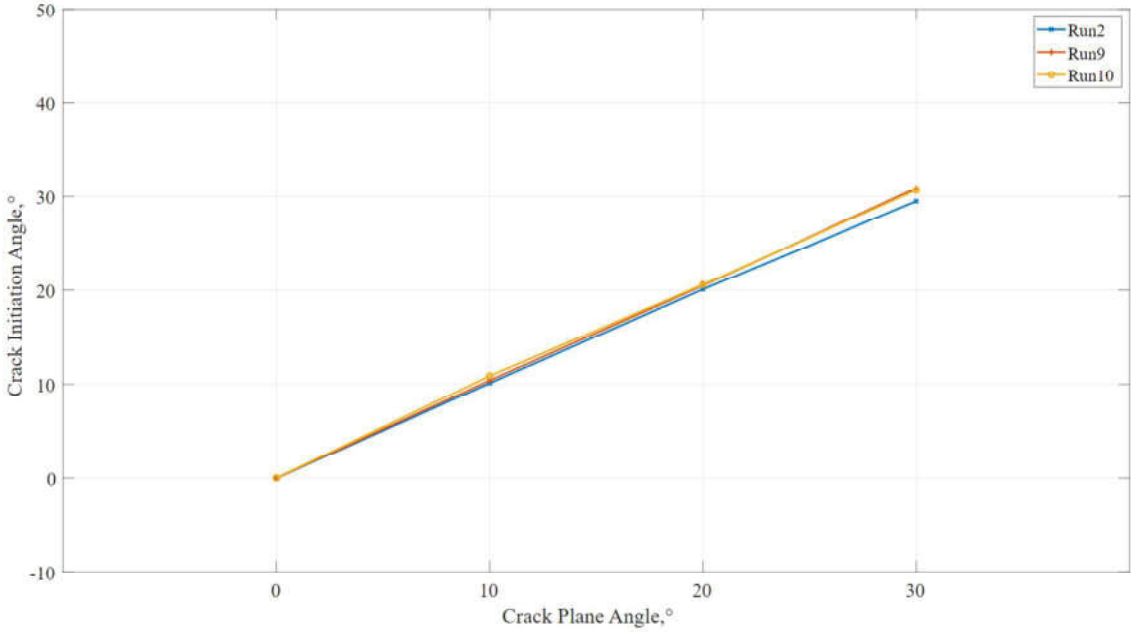

Figure 4.9. Crack initiation angles according to Ip criterion to evaluate effect of transformation start stress levels.

4.4. Martensitic Volume Fraction (mvf) Contours Interpretation

In order to evaluate the stress induced phase transformation phenomena which is unique for SMA, the martensitic volume fractions are extracted from ABAQUS for each node and plotted using MATLAB software. The results of the plots and effect on the crack initiation angle are interpreted in the Discussion.

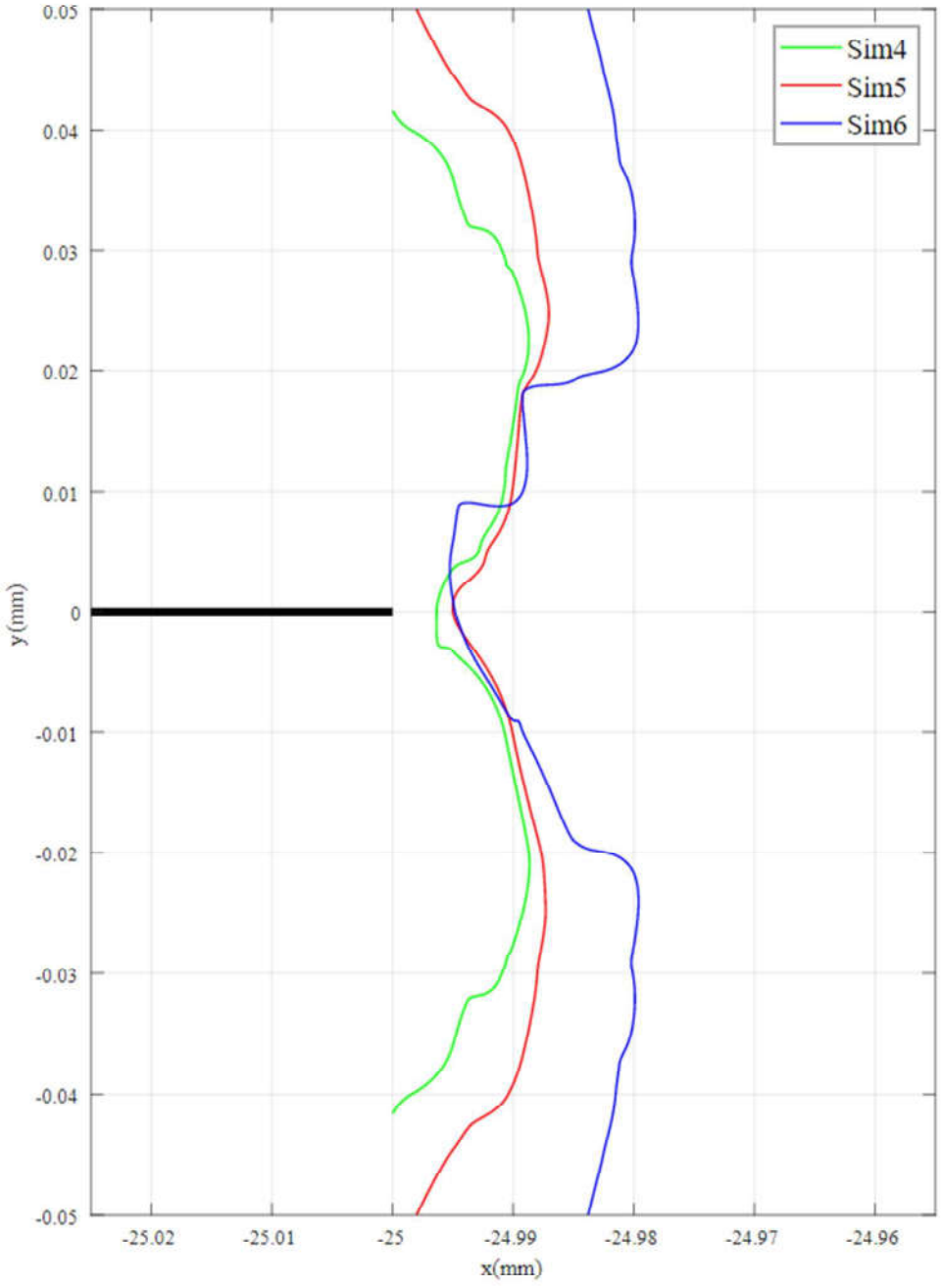

Figure 4.10. mvf for 0° crack plane for Sim 4, Sim 5, Sim 6.

As it can be seen through Figure 4.10, the mvf is increasing with the decreasing transformation strain for Sim 4, Sim 5 and Sim 6. Higher transformation strain will generate longer strain pletau between σ^{MS} and σ^{MF} which makes harder to fully transform austenite. Additionally, since the crack angle is 0° for Figure 4.10, the symmetry of the mvf with respect to x axis is observed especially for Sim 4 and Sim 5.

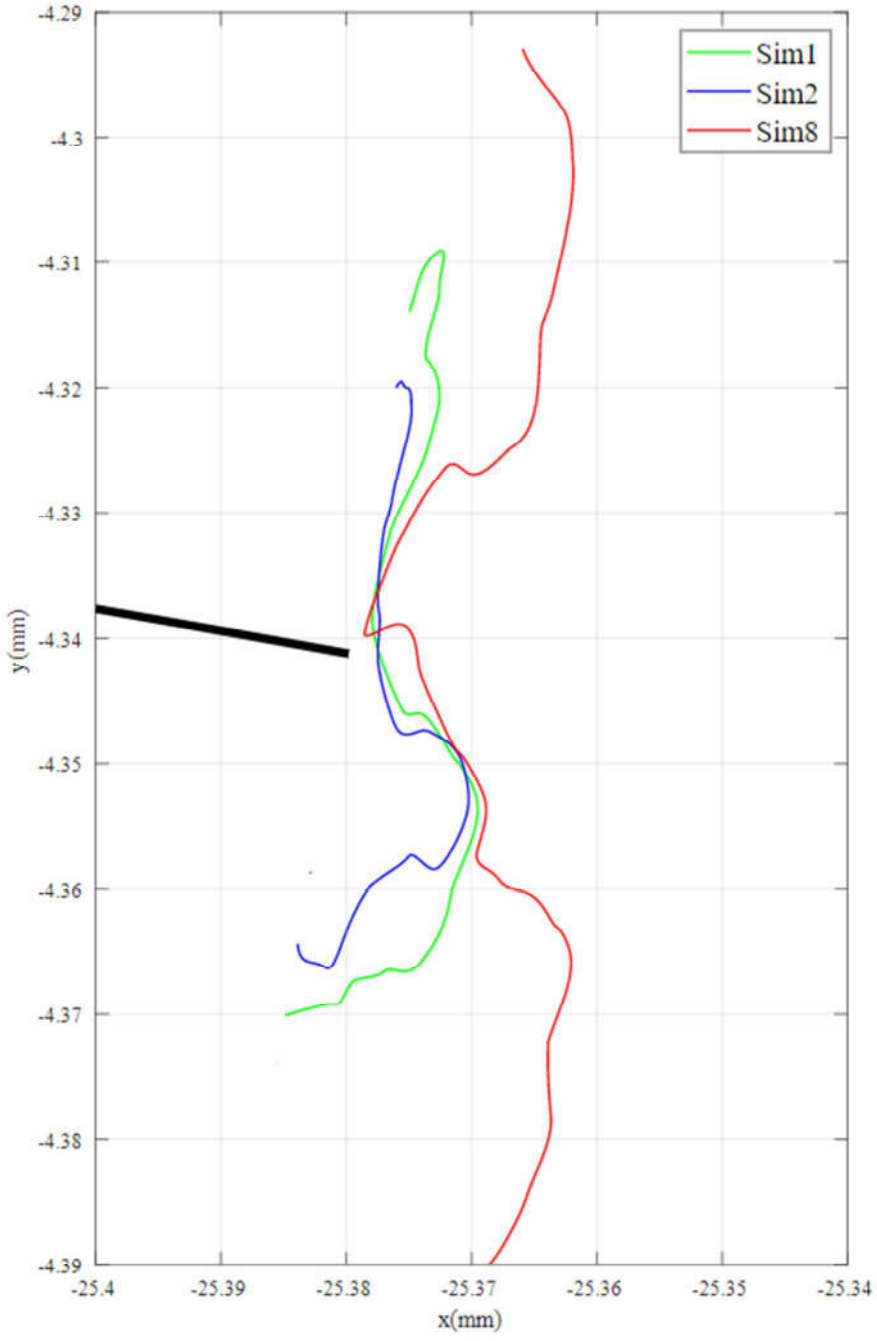

Figure 4.11. mvf for 10° crack plane for Sim 1, Sim 2, Sim 8.

The second sub-simulation group (Figure 4.11) for transformation strain is in good agreement with the first sub-simulation group (Figure 4.10) as the mvf is increasing with the decreasing transformation strain.

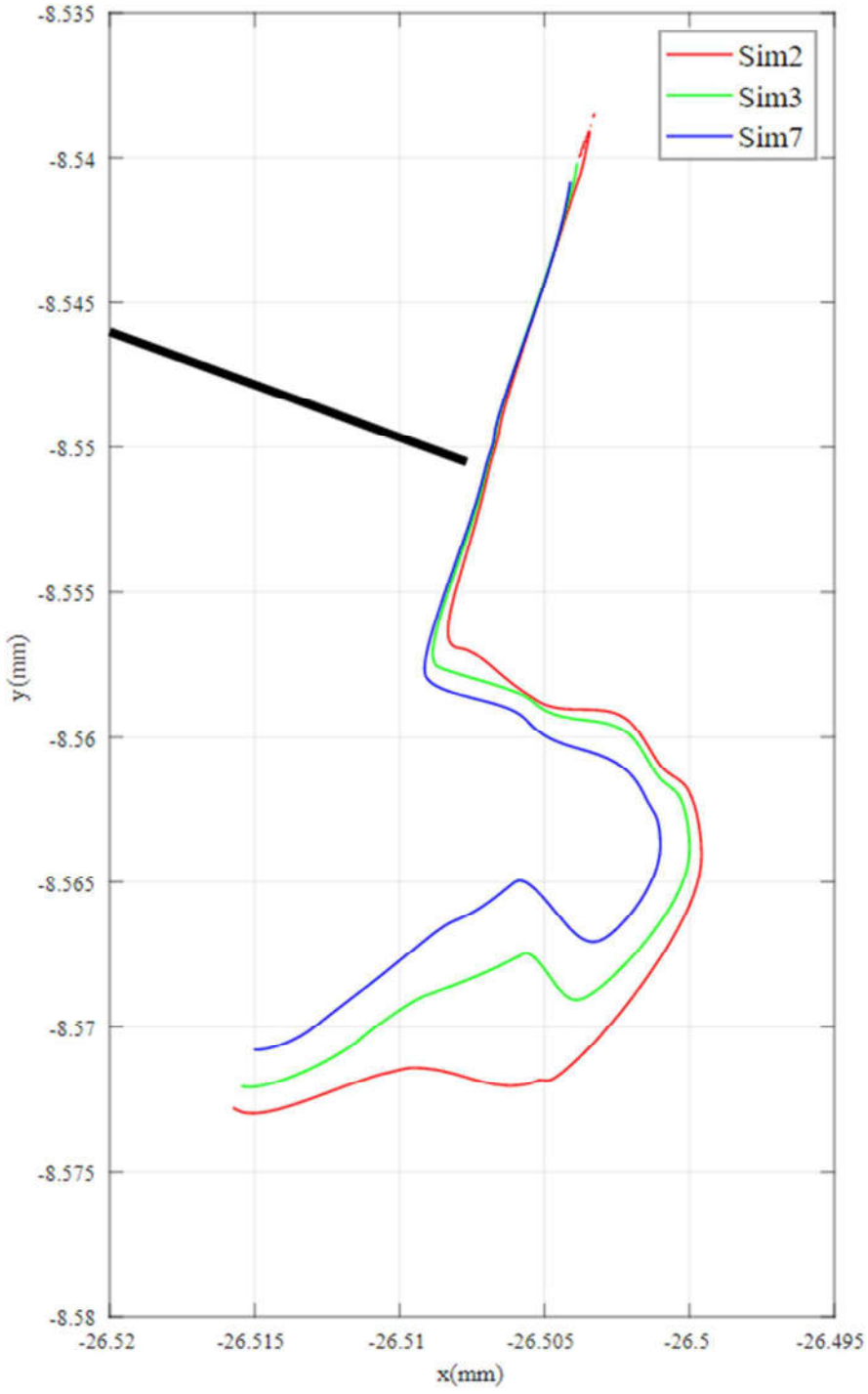

Figure 4.12. mvf for 20° crack plane for Sim 2, Sim 3, Sim 7.

As it can be seen through Figure 4.12, the mvf is increasing with decreasing transformation finish stress for Sim 2, Sim 3 and Sim 7. This can be interpreted as due to high σ^{MF}, the stress required to achieve fully martensitic zone is harder to reach. The fully martensitic zone on the upper half of the crack tip is not totally observed because of it is not in the nodal range of the previously defined paths.

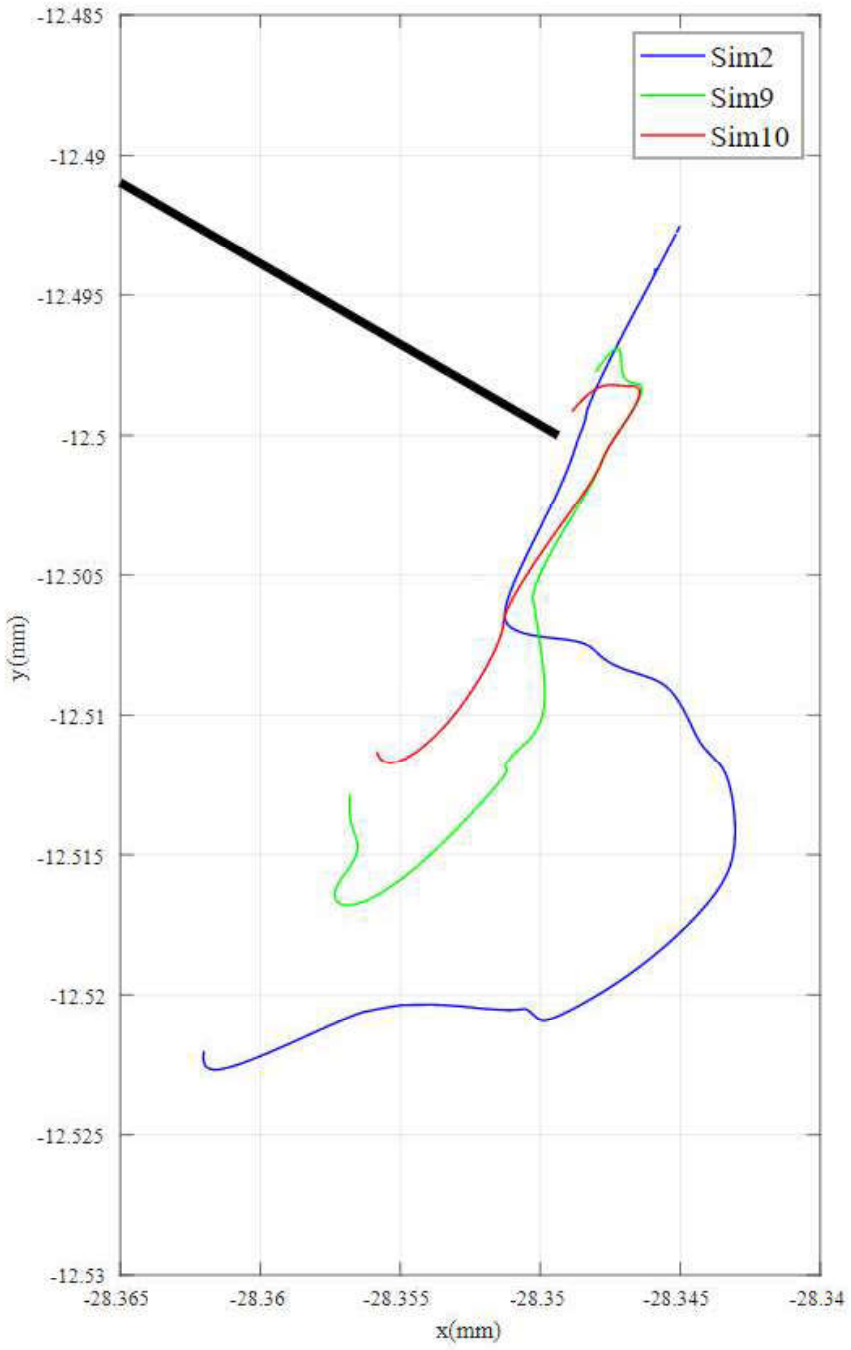

Figure 4.13. mvf for 30° crack plane for Sim 2, Sim 9, Sim 10.

The mvf is increasing with the decreasing transformation start stress level for Sim 2, Sim 9 and Sim 10. The stress required to start and end the transformation is high when stress level is high. Therefore, fully transforming material is harder with the equivalent loading between the simulations. The upper half of the fully martensitic zone is not observed similarly to the Figure 4.12.

The stress parallel to the crack faces is defined as T stress. It is used to introduce the effect of core region radius, r_c, on the crack initiation angle. As core region radius varies under mixed mode loading, the T stress has an unelidable effect on tangential stress and therefore crack initiation angle. Therefore, effect of the T stress introduced in MTS criterion and named as Generalized-MTS (GMTS) by Williams and Ewing[62]. The T Stress values regarding all simulations are given in the Figure 4.15 for further studies regarding the GMTS.

The J Integral values are plotted in the following Figure 4.14 for all simulations. The results of the J Integral cannot be directly related to the change in fully martensitic zone between the simulations. Therefore, the crack initiation angle is not studied in terms of the J Integral. The J Integral values shown in the Figure 4.14 are taken for same path for every simulation. However, the results may vary for each simulation since the J Integral is path dependent as shown by Baxevanis [63] due to energy dissipations. The correct path in order to evaluate the crack behavior may change for each simulation, therefore this phenomenon should be studied separately.

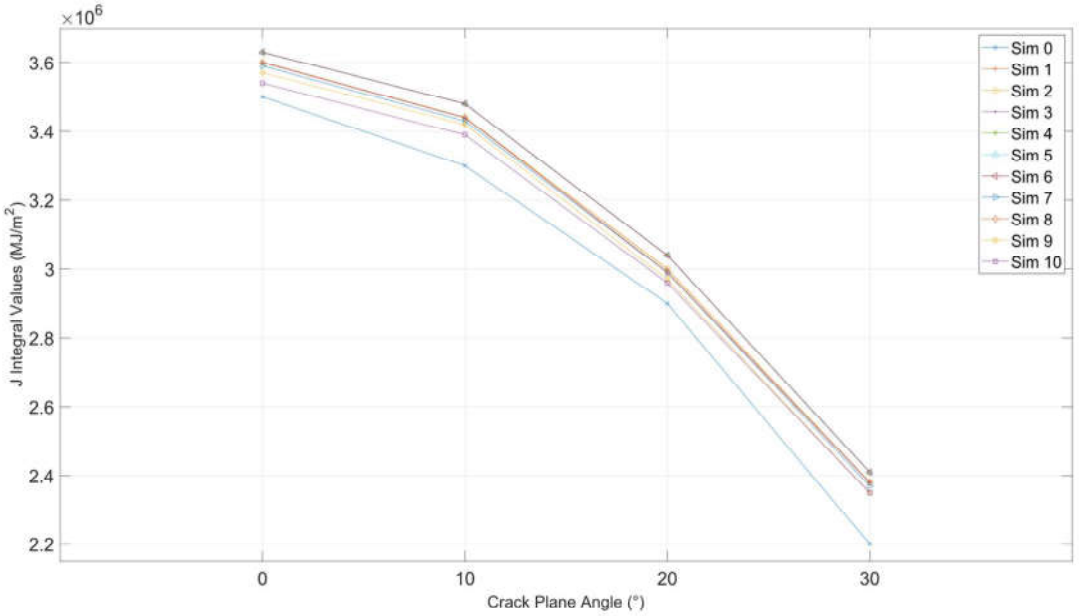

Figure 4.14. The J Integral values.

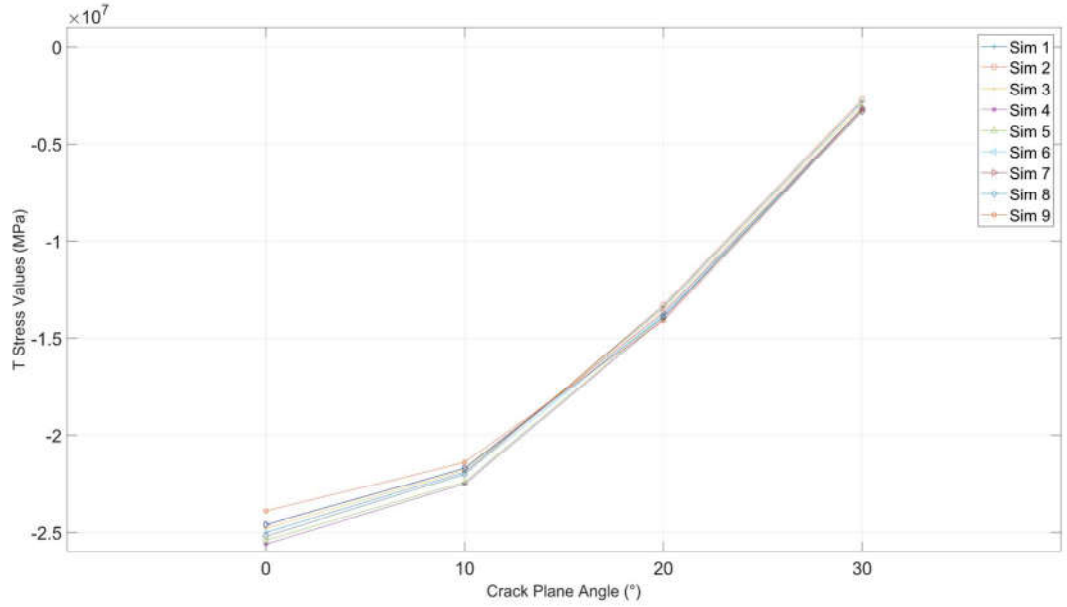

Figure 4.15. The T stress values.

5. DISCUSSION

In the light of the above explained results, the behavior of crack initiations is compared for different material properties. The crack initiation angle results, mvf graphs that are given in the previous chapter are discussed and related to the toughening mechanism of the crack. In which way the fully martensitic zone effects the behavior of the crack initiation angle is interpreted. In order to that, simulation groups are formed as in Results Section and the observed results for each simulation group are studied in cause effect relationship. Additionally, effect of the crack plane angle on crack initiation angle is discussed further by examining the different angle mvf graphs for each simulation group.

Since the main aim of the thesis is to understand the effect of SMA crack initiation behavior, the stress induced martensitic transformation is investigated. The size and shape of the martensitic zone near crack tip shall be identified in order to understand its effect on crack. Therefore, the size of martensitic transformed zone shall be evaluated for different crack angles and different material properties. The martensitic transformation near the crack tip is studied in the literature by Sung Yi et al. and the results in this thesis are in good agreement with his paper [64].

The fully martensitic region is obtained when the stress applied is above the σ^{MF}. The outer zone represents the partially transformed and fully austenitic regions. The limit between austenite and partially transformed region is separated by σ^{MS} but since the aim of the thesis is to define behavior of martensitic region, so called zones are not studied. Therefore, with limited number of nodal points near crack tip, calculations are done more efficiently for the evaluation of fully martensitic zone.

In the results section, the limits for the fully martensitic region are determined. The boundaries that are represented in the Figures 4.10, 4.11, 4.12 and 4.13 are called transformation finish curve. The martensitic transformed zone size is increasing with the increasing crack angle. So, it can be said that by increasing Mode II loading, the transformation zone also increases. The deviations in the angles are interpreted in terms of phase transformation changes below.

In the literature, this effect is referred as (martensitic) transformation toughening. Therefore, the transformation strain, start of transformation and end of transformation stresses are changed between simulations, aiming to change the size of martensitic zone around the crack tip. The effect of the fracture toughness is studied by Lagoudas et al. [65] by using thermomechanical and temperature parameters modelled on FE model and his computations show that fracture toughness is increased in the wake of crack growing crack where the fully martensitic zone is present. Another study regarding experimental and computational investigation of the phase transformation effect on fracture parameters of SMA is studied by Haghgouyan et al. [66] by modeling the two simulations which differs in terms of lack of phase transformation. He showed that critical stress intensity factor is changing for transforming specimen and therefore this phenomenon corroborates the toughening effect by the authors. Baxevanis et al. [63] showed that the transformation zone dependent to the ratio of the Young's moduli of martensite and austenite and it is observed that increase in the transformation size contributes to the toughness. Moreover, the J Integral is found to be path dependent between far field and crack tip.

The stress initiation criterions are evaluated in terms of 5 criterions. The results show that MTS, Det and Ip criterion show comparable results however the S and T criterion results shall be studied further since the results are not in line with the general tendency of crack growth.

The impact of the transformation finish stress is evaluated from the Sim 2, Sim 3 and Sim 7. Under same experimental parameters, the martensitic transformation is aimed to decrease between these simulations respectively, since more stress is required to transform material from austenitic phase to martensitic phase. The ABAQUS results also verify the decreasing mvf ratio between simulations as it can be seen on Figures 4.10, 4.11, 4.12 and 4.13.

The MTS criterion results shows small deviations that can be related to the crack tip phase transformation effect. It shall be underlined that small deviations from the crack plane are increasing with the increasing crack angle. However, even though small deviations are present, the crack initiation angles tend to not coincide with the martensitic region.

Therefore, it is interpreted as effect of hardening of the martensitic region. The lowest martensite present simulation, so the lowest super elastic behavior, is present in Sim7 between 3 simulations. Similarly, in terms of the crack angles, the highest deviation from the crack plane is observed in Sim 7. The Det and Ip criterions show very small differences and it is hard to see the effect of martensitic transformation. Even though graphs show similar shapes and supports the results in MTS Criterion, the differences between simulations are negligibly small and may be further studied.

The effect of the transformation start stress level is investigated by the Sim 2, Sim 9 and Sim 10. The martensitic deformation is controlled by implementing high stress levels that can transform material to martensite totally in a very small zone compared to the other simulations. Therefore, the martensitic transformation is very limited on the higher transformation levels. As a consequence, Sim 10 represents the lowest super elastic behavior material between all simulations. The results are consistent with the results of Sung Yi et al.[62].

It is observed that, the effect of fully transferred martensitic zone is similar to the results of the end stress transformation simulations. The MTS criterion values shall be interpreted in terms of martensitic transformation since there are significant differences present between simulations. The Sim 2 is deviating from the crack plane less than the other 2 simulations which are the lowest mvf value obtained simulations. This behavior shows that the increasing mvf makes crack to initiate from a significantly less deviated angle. The Det and Ip criterion results are relatively close to each other however, it is not correct to comment on the results as the minimal differences may be considered inside error tolerances of the simulations. Nevertheless, the results support the MTS Criterion since the evaluated crack initiation values are in the same order.

The effect of the transformation strain is studied twice with two different simulation groups as first group is consisting of Sim 4, Sim 5, Sim 6 and second group is consisting of Sim 1, Sim 2 and Sim 8. When the mvf values are investigated, it is seen that with the lowest transformation stress level and the lowest transformation strain, Sim 6 specimen has the largest martensitic zone. Therefore, Sim 6 is the best option in order to investigate the martensitic behavior that is present in the crack tip.

The 2 simulation group results are consistent among them. It is observed that the martensitic deformation is inversely proportional to the transformation strain. The results are again in line with the other simulation group results that are with increasing the martensitic transformation zone around the crack tip, the crack initiation tend to deviate less from the crack plane angle according to MTS direction. The Det and Ip criterions give similar results that are relatively small for the evaluation. However, the graphs are similar to MTS Criterion with margins are minimized between simulations as represented in the Figures 4.7 and 4.8. Therefore, highest deviation from the crack plane is observed in the Sim 4 and similarly, in the Sim 2 for the other simulation group.

For comparison purposes, the linear elastic model also studied as an $\zeta=0$ simulation (Sim 0). The Sim 0 crack initiation curve is above all other curves for every crack initiation parameter. As an example, the lowest mvf simulation, Sim 10 can be compared to Sim 0 for the 30° crack angle, in which the effect of the toughening effect observed more easily. The Sim 10 crack initiation angle are 42°, 32° and 32° for the MTS, Det and Ip criterions, respectively. On the other hand, the crack initiation angles for the linear elastic material are found to be 45°, 33° and 34°. The linear elastic model shows higher deviation from the crack plane angle and even with very small fully martensitic region in the Sim 10, the toughening effect is observed compared Sim 0. Additionally, Sim 6 shows the most toughening effect since the mvf ratio is the highest. The crack initiation angles for the Sim 6 are 32°, 30° and 30° for the MTS, Det and Ip criterions, respectively for the 30° crack plane. The difference between crack initiation angles is more obvious between Sim 0 and Sim 6. Therefore, it should be interpreted as, the toughening mechanism on SMA is affecting the crack angle with the observed results. These results are in good agreement with the interpretation made for other 4 simulation groups.

In terms of material changes, the discussion is finalized as follows. With the help of all mentioned results and interpretations, the observed result is that martensitic transformation effects the crack initiation angle according to simulations especially in terms of MTS Criterion. The crack tends to initiate less from the martensitic dense zones and pushed towards 0° angle with respect to crack plane-oriented reference system. The outer zone of the martensitic transformation curve is consisting of A and M phases and crack tends to initiate from transformation zone. This phenomenon shall be considered as evidence for

toughening mechanism due to stress induced martensitic transformation and its effects on crack initiation.

It is observed that the critical crack angle is increasing with crack plane angle according to MTS criterion. However, according to Det and Ip Criterions, the differences between crack plane angle and critical crack angle is not more than 1°-2°. Therefore, the effect of the crack plane angle on critical crack angle is observed as negligible. The phase angle (crack plane angle) effect is studied by Freed et al. and their study showed that an increasing value of phase angle yields a larger transformation zone [67] which supports the results obtained in the Figures 4.10, 4.11, 4.12 and 4.13.

6. CONCLUSION

The fracture of SMA shall be investigated in different zones. The LEFM is sufficient to evaluate fractures in the austenitic zones. The transformation zone, which includes both austenite and martensite phases is evaluated by the HRR fields in the literature and crack initiations are interpreted. In this thesis, the fully martensitic zones are mainly studied. The effects of the martensitic region on the crack initiation are aimed to be discussed.

The FEA method, on ABAQUS software, is used to simulate different crack angles and different materials. The 0°, 10°, 20° and 30° angles are studied and the stress, strain, mvf, strain energy density and nodal coordinates are extracted to study crack initiation criterions. Despite the studies in the literature, instead of analytic models to calculate the required parameters for each crack initiation, the ABAQUS values are processed.

An obstacle to use ABAQUS values directly is the non-continuous nodal values. This obstacle is solved by processing data values on the MATLAB to obtain a continuous function. The least square nonlinear fit regression is implemented for such purposes. Fitting is verified by obtaining very accurate results with the equivalent nodal ABAQUS values.

5 criterions are evaluated to obtain crack initiation angles for Simulations. MTS, Det and Ip criterions are coinciding among them. However, the S Criterion and T Criterion results are obtained inaccurately and therefore they should be further studied to be compared with the other criterions.

In the results section, the crack initiation angles on the above explained 3 criterions are plotted in small simulation groups in order to understand the effect of the different material properties such as transformation finish stress, transformations start stress levels and transformation strain. In addition, the mvf graphs are plotted for interpreting on effect of the martensitic region size and shape on the crack initiation angle.

Result showed that martensitic region is affecting the crack angle in a minor way especially in terms of MTS Criterion. The Det and Ip Criterion is supporting the MTS

Criterion however differences are minimal compared to MTS Criterion. To conclude, it is observed that increasing martensitic transformed zone by different material properties resulted with the crack tendency to initiate from 0° with respect to crack plane.

,

REFERENCES

1. Buehler, W. J., J. V. Gilfrich and R. C. Wiley, "Effects of Low-Temperature Phase Changes on the Mechanical Properties of Alloys Near Composition NiTi", *Journal of Applied Physics*, Vol. 34, pp. 1465-1477, 1963.

2. Miyazaki, S., K. Otsuka and Y. Suzuki, "Transformation Pseudoelasticity and Deformation Behavior in a Ti-50.6at%Ni Alloy", *Scripta Materialia*, pp. 287–292, 1972.

3. Tadaki, T., K. Otsuka and K. Shimizu, "Shape Memory Alloys", *Annual Review of Materials Science*, Vol. 18, pp. 25-45, 1988.

4. Karagoz, Z. and C. A. Canbay, "Relationship Between Transformation Temperatures and Alloying Elements in Cu–Al–Ni Shape Memory Alloys", Springer, Hungary, 2013.

5. Hartl, D. J. and D. C. Lagoudas, "Aerospace Applications of Shape Memory Alloys", *Proceedings of the Institution of Mechanical Engineers, Part G: Journal of Aerospace Engineering*, Vol. 221, pp. 535-552, 2007.

6. Chang, W.S. and Y. Araki, "Use of Shape-Memory Alloys in Construction: A Critical Review", *Proceedings of the Institution of Civil Engineers-Civil Engineering,* Vol. 169, No. 2, Thomas Telford Ltd, 2016.

7. Lendlein, A. and K. Steffen, "Shape-Memory Polymers", *Angewandte Chemie International Edition*, Vol. 41, No. 12, pp. 2034-2057, 2002.

8. Stoeckel, D., "Shape Memory Actuators for Automotive Applications", *Materials & Design*, Vol. 11, pp. 302-307, 1990.

9. Liang, C. and C. A. Rogers, "Design of Shape Memory Alloy Actuators", *Journal of Mechanical Design*, Vol. 114, pp. 223-230, 1992.

10. Tong, H. C. and C. M. Wayman, "Characteristic Temperatures and Other Properties of Thermoelastic Martensite", *Acta Metallurgica*, Vol. 22, No. 7, pp. 887-896, 1974.

11. Otsuka, K., "Crystallography of Martensitic Transformations and Lattice Invariant Shears", *Materials Science Forum*, Trans Tech Publications Ltd, 1990.

12. Lu, Z. K. and G. J. Weng., "Martensitic Transformation and Stress-Strain Relations of Shape-Memory Alloys", *Journal of the Mechanics and Physics of Solids*, Vol. 45, pp. 1905-1928, 1997.

13. Anderson, T. L., "*Fracture Mechanics: Fundamentals and Applications*", CRC Press, 2017.

14. Popov, P. and D. C. Lagoudas, "A 3-D Constitutive Model for Shape Memory Alloys Incorporating Pseudoelasticity and Detwinning of Self-Accommodated Martensite", *International Journal of Plasticity*, Vol. 23, pp. 1679-1720, 2007.

15. Patoor, E. and D. C. Lagoudas, "Shape Memory Alloys, Part I: General Properties and Modeling of Single Crystals", *Mechanics of Materials*, Vol. 18, pp. 391-429, 2006.

16. Stepanova, L. and P. Roslyakov, "Complete Williams Asymptotic Expansion of the Stress Field Near the Crack Tip: Analytical Solutions, Interference-Optic Methods and Numerical Experiments", *AIP Conference Proceedings*, Vol. 1785, No. 1, AIP Publishing LLC, 2016.

17. Hutchinson, J. W. and Z. Suo., "Mixed Mode Cracking in Layered Materials", *Advances in Applied Mechanics*, Vol. 29, Elsevier, pp. 63-191, 1991.

18. Griffith, A., "VI. The Phenomena of Rupture and Flow in Solids", *Philosophical Transactions of The Royal Society of London, Series A, Containing Papers of a Mathematical or Physical Character*, Vol. 221, pp. 163-198, 1921.

19. Sih, G. C. "Energy-Density Concept in Fracture Mechanics", *Engineering Fracture Mechanic*s, Vol. 5, pp. 1037-1040, 1973.

20. Hill, R., "The Mathematical Theory of Plasticity, Clarendon" Oxford, Vol. 11, pp. 613-614, 1950.

21. Hill, R. and J. Rice, "Elastic Potentials and The Structure of Inelastic Constitutive Laws", *SIAM Journal on Applied Mathematics*, Vol. 25, pp. 448-461, 1973.

22. Dryden, H. L., T. Von Kármán, G. Kuerti, F.H. Van Den Dungen, L. Howarth and J. Peres, "Advances in Applied Mechanics", Academic Press, 1958.

23. Williams, M. L., "The Stresses Around a Fault or Crack in Dissimilar Media", *Bulletin of The Seismological Society of America*, Vol. 49, pp. 199-204, 1959.

24. Rice, J. R., "Contained Plastic Deformation Near Cracks and Notches Under Longitudinal Shear", *International Journal of Fracture Mechanics*, Vol. 2, pp. 426-447, 1966.

25. Raju, I. S. and J. C. Newman Jr., "Stress-Intensity Factors for Internal and External Surface Cracks in Cylindrical Vessels", *Journal of Pressure Vessel Technology*, pp. 293-298, 1982.

26. Maletta, C. and F. Furgiuele, "Analytical Modeling of Stress-Induced Martensitic Transformation in The Crack Tip Region of Nickel–Titanium Alloys", *Acta Materialia*, Vol. 58, pp. 92-101, 2010.

27. Maletta, C., E. Sgambitterra and F. Furgiuele, “Crack Tip Stress Distribution and Stress Intensity Factor in Shape Memory Alloys”, *Fatigue & Fracture of Engineering Materials & Structures*, Vol. 36, pp. 903-912, 2013.

28. Hui, C. Y. and H. Riedel, “The Asymptotic Stress and Strain Field Near the Tip of a Growing Crack Under Creep Conditions”, *International Journal of Fracture*, Vol. 17, pp. 409-425, 1981.

29. Williams, Max L., “On the Stress Distribution at the Base of a Stationary Crack”, *Journal of Applied Mechanics*, Vol. 24, pp. 109-114, 1957.

30. Özerim, G., G. Anlaş and Z., Moumni, “On Crack Tip Stress Fields in Pseudoelastic Shape Memory Alloys”, *International Journal of Fracture*, pp. 205-217, 2018.

31. Zaki, W. and Z. Moumni, “A Three-Dimensional Model of The Thermomechanical Behavior of Shape Memory Alloys”, *Journal of the Mechanics and Physics of Solids*, Vol. 55, pp. 2455-2490, 2007.

32. Auricchio, F. and R.L. Taylor, “Shape-Memory Alloys: Modeling and Numerical Simulations of the Finite-Strain Superelastic Behavior”, *Computer Methods in Applied Mechanics and Engineering*, Vol. 143, pp. 175–194, 1996.

33. Auricchio, F. and J. Lubliner, “Shape-Memory Alloys: Macro-modelling and Numerical Simulations of the Superelastic Behavior”, *Computer Methods in Applied Mechanics and Engineering*, Vol. 146, pp. 281–312, 1997.

34. ABAQUS, *User Manual, Superelasticity,* https://ABAQUS-docs.mit.edu/2017 /English/SIMACAEMATRefMap/simamat-c-superelasticity.htm, accessed in December 2021.

35. Mutlu, F., *Effect of Loading Rate on Fracture of NiTi*, Master’s Thesis, Boğaziçi University, 2016.

36. Gu, Xiaojun, “Time Integration and Assessment of a Model for Shape Memory Alloys Considering Multiaxial Nonproportional Loading Cases”, *International Journal of Solids and Structures*, Vol. 54, pp. 82-99, 2015.

37. Özerim, G., *Evaluation of Crack Tip Singular Fields in Shape Memory Alloys*, Master’s Thesis, Boğaziçi University, 2017.

38. Shirangi, M. G. and A. A. Emerick, “An Improved TSVD-Based Levenberg–Marquardt Algorithm for History Matching and Comparison with Gauss–Newton”, *Journal of Petroleum Science and Engineering,* Vol. 143, pp. 258-271, 2016.

39. Gallant, A.R., “Nonlinear Regression”, *The American Statistician*, Vol. 29, pp. 73-81, 1975.

40. MATHWORKS, User Manual – Nonlinear Regression, https://www.mathworks.com/help/optim/ug/lsqnonlin.html, accessed in November 2021.

41. Chapra, S. C. and R. P. Canale, *Numerical Methods for Engineers*, Vol. 1221, New York: McGraw-Hill, 2011.

42. Moré, J. J., “The Levenberg-Marquardt Algorithm: Implementation and Theory”, *Numerical Analysis*, Springer, Berlin, Heidelberg, pp. 105-116, 1978.

43. Curry, H. B., “The Method of Steepest Descent for Non-Linear Minimization Problems”, *Quarterly of Applied Mathematics*, Vol. 2, pp. 258-261, 1944.

44. Gratton, S., A. S. Lawless and N. K. Nichols, “Approximate Gauss–Newton Methods for Nonlinear Least Squares Problems”, *SIAM Journal on Optimization*, Vol. 18, pp. 106-132, 2007.

45. Guillaume, P. and R. Pintelon, “A Gauss-Newton-Like Optimization Algorithm for Weighted Nonlinear Least-Squares Problems”, *IEEE Transactions on Signal Processing*, Vol. 44, pp. 2222-2228, 1996.

46. Marquardt, D., “An Algorithm for Least-squares Estimation of Nonlinear Parameters”, *SIAM Journal Applied Mathematics*, Vol. 11, pp. 431–441, 1963.

47. Levenberg, K., “A Method for the Solution of Certain Problems in Least-Squares”, *Quarterly Applied Mathematics,* Vol. 2, pp. 164–168, 1944.

48. Moré, J. J., B. S. Garbow and K. E. Hillstrom, *User Guide for MINPACK 1*, Argonne National Laboratory, Rept. ANL–80–74, 1980.

49. Erdogan, F. and G. C. Sih, “On the Crack Extension in Plates Under Plane Loading and Transverse Shear”, *Journal of Basic Engineering*, Vol. 85, pp. 519-525, 1963.

50. Sih, George C., *Methods of Analysis and Solution of Crack Problems: Recent Developments in Fracture Mechanics, Theory and Methods of Solving Crack Problems*, Noordhoff International Publishing, 1973.

51. Vallejo, L. E., “The Brittle and Ductile Behavior of Clay Samples Containing a Crack Under Mixed Mode Loading”, *Theoretical and Applied Fracture Mechanics*, Vol. 10, pp. 73-78, 1988.

52. Hussain, M. A., L. Pu and J. Underwood, “Strain Energy Release Rate”, *Proceedings of the 1973 National Symposium on Fracture Mechanics*, Vol. 559, 1974.

53. Sih, G. C., “Strain-Energy-Density Factor Applied to Mixed Mode Crack Problems”, *International Journal of Fracture*, Vol. 10, pp. 305-321, 1974.

54. Gandelsman, M., “Strain Energy in Uniaxial Loads”, *Engineering Mechanics*, UNL College of Engineering and Technology, 1999.

55. Theocaris, P. S. and N. P. Andrianopoulos, “The Mises Elastic-Plastic Boundary as the Core Region in Fracture Criteria”, *Engineering Fracture Mechanics*, Vol. 16, pp. 425-432, 1982.

56. Theocaris, P. S., G. A. Kardomateas and N. P. Andrianopoulos, "Experimental Study of the T-Criterion in Ductile Fractures", *Engineering Fracture Mechanics*, Vol. 17, pp. 439-447, 1983.

57. Theocaris, P. S., "A Higher-Order Approximation for the T-criterion of Fracture in Biaxial Fields", *Engineering Fracture Mechanics*, Vol. 19, No. 6, pp. 975-991, 1984.

58. Papadopoulos, G. A., "The Stationary Value of the Third Stress Invariant as a Local Fracture Parameter (Det.-criterion)", *Engineering Fracture Mechanics*, Vol. 27, pp. 643-652, 1987.

59. Papadopoulos, G. A., "Experimental Det.-Criterion of Fracture", *Fracture Mechanics*, Springer, pp. 269-272, 1993.

60. Papadopoulos, G. A., "Fracture Mechanics: The Experimental Method of Caustics and the Det.-Criterion of Fracture", Springer Science & Business Media, 2012.

61. Ukadgaonker, V. G. and P. J. Awasare, "A New Criterion for Fracture Initiation", *Engineering Fracture Mechanics*, Vol. 51, pp. 265-274, 1995.

62. Williams, J. G. and P. D. Ewing, "Fracture Under Complex Stress the Angled Crack Problem", *Int J Fract Mech*, Vol. 8, pp. 441-446, 1972.

63. Baxevanis, T., Y. Chemisky and D. C. Lagoudas, "Finite Element Analysis of the Plane Strain Crack-Tip Mechanical Fields in Pseudoelastic Shape Memory Alloys", *Smart Materials and Structures*, Vol. 21, 2012.

64. Yi, S., S. Gao and L. Shen, "Fracture Toughening Mechanism of Shape Memory Alloys Under Mixed-Mode Loading Due to Martensite Transformation", *International Journal of Solids and Structures*, Vol. 38, pp. 4463-4476, 2001.

65. Baxevanis, T., C. M. Landis and D. C. Lagoudas, “On the Fracture Toughness of Pseudoelastic Shape Memory Alloys”, *Journal of Applied Mechanics*, Vol. 81, 2014.

66. Haghgouyan, B., N. Shafaghi, C.C. Aydıner and G. Anlas, “Experimental and Computational Investigation of the Effect of Phase Transformation on Fracture Parameters of a SMA”, *Smart Materials and Structures*, Vol. 25, 2016.

67. Freed, Y., L. Banks-Sills and J. Aboudi, “On the Transformation Toughening of a Crack Along an Interface Between a Shape Memory Alloy and an Isotropic Medium”, *Journal of the Mechanics and Physics of Solids*, Vol. 56, pp. 3003-3020, 2008.